Author Manuscript

Author Manuscript

Author Manuscript

Author Manuscript

HHS Public Access

Author manuscript

Cell Rep. Author manuscript; available in PMC 2022 April 04.

Published in final edited form as:

Cell Rep. 2021 November 23; 37(8): 110059. doi:10.1016/j.celrep.2021.110059.

Loop extrusion promotes an alternate pathway for isotype switching

Hong Ming Shen[1], **Robert Wuerffel**[1,4], **Jose F. Cantillo**[1,5], **Saurabh Priyadarshi**[1], **Xue Lei**[2,6], **Jie Liang**[2], **Yee Ling Wu**[3], **Amy L. Kenter**[1,7,*]

[1]Department of Microbiology and Immunology, University of Illinois College of Medicine, Chicago, IL 60612-7344, USA

[2]Department of Bioengineering, University of Illinois Colleges of Engineering and Medicine, Chicago, IL 60612-7344, USA

[3]Department of Microbiology and Immunology, Loyola University Chicago, Maywood, IL 60153, USA

[4]Present address: 10441 Circle Drive, Apartment 47C, Oak Lawn, IL 60453, USA

[5]Present address: Inmunotek, S.L., Alcalá de Henares, Spain

[6]Present address: Sanford Burnham Prebys Medical Discovery Institute, La Jolla, CA 92037, USA

[7]Lead contact

SUMMARY

Class-switch recombination (CSR) involves replacement of the Cμ constant region with another downstream C_H region. CSR is initiated by activation-induced cytidine deaminase (AID)-mediated DNA breaks that are targeted to transcriptionally active switch (S) regions. S region promoters (Prs) direct synapsis by associating with the Eμ and 3′Eα enhancers that jointly anchor a chromatin loop. We report that asymmetric loop extrusion allows 3′Eα to track along the locus and form Pr-Pr-E interactions that mediate CSR between downstream S regions, followed by switching to donor Sμ. This alternative pathway bypasses sequential switching and creates immunoglobulin (Ig)E^+ B cells in the absence of IgG1 expression. Based on the analysis of diagnostic CSR products in B cell subsets, we identify a BCR-negative cell intermediate that is pivotal to efficient CSR.

Graphical abstract

This is an open access article under the CC BY-NC-ND license (http://creativecommons.org/licenses/by-nc-nd/4.0/).

*Correspondence: star1@uic.edu.

AUTHOR CONTRIBUTIONS

Conceptualization, A.L.K. and H.M.S.; methodology, R.W., X.L., J.L., and A.L.K.; validation, H.M.S., R.W., and J.F.C.; investigation, H.M.S., R.W., S.P., and J.F.C.; formal analysis, X.L. and J.L.; resources, A.L.K. and Y.L.W.; writing – original draft, A.L.K.; writing – review and editing, H.M.S. and J.F.C.; visualization, H.M.S., X.L., J.F.C., and A.L.K.; supervision, project administration, and funding acquisition, A.L.K.

SUPPLEMENTAL INFORMATION

Supplemental information can be found online at https://doi.org/10.1016/j.celrep.2021.110059.

DECLARATION OF INTERESTS

The authors declare no competing interests.

Author Manuscript Author Manuscript Author Manuscript Author Manuscript

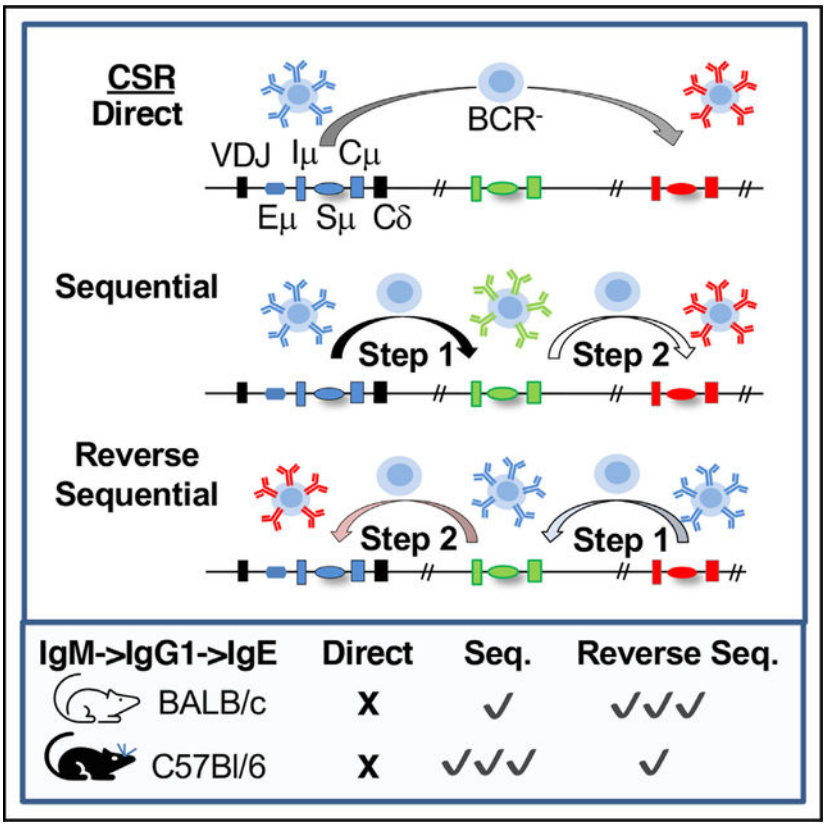

In brief

Shen et al. report that 3′Eα tracks along the Igh locus via unidirectional loop extrusion to form germline transcript promoter (Pr)-Pr-E interactions that mediate an alternative CSR pathway. B cell intermediates of CSR are identified, which are AID-dependent, surface BCR-negative, and in the G_1 phase of the cell cycle.

INTRODUCTION

Immunoglobulin (Ig) class-switch recombination (CSR) diver-sifies Ig effector function to optimize humoral immune responses. The mouse *Igh* locus contains eight C_H genes (μ, δ, γ3, γ1, γ2b, γ2a, ε, and α) that are located downstream of the V, D, and J segments and are bracketed by the Eμ and 3′Eα enhancers. C_H genes are organized as transcription units composed of a germline transcript (GLT) promoter (Pr), I (intervening) exon, and long repetitive switch (S) region upstream of each C_H gene (except Cδ). CSR occurs through an intra-chromosomal deletional mechanism that involves the joining of activation-induced cytidine deaminase (AID)-induced double-strand breaks (DSBs) in the donor Sμ and a downstream S region and generation of Sμ-Sx hybrid junctions. The C_H region domain is encompassed by a large chromatin loop that is anchored by the distantly located enhancers, Eμ and 3′Eα (Dong et al., 2015; Feldman et al., 2015; Sellars et al., 2009; Wuerffel et al., 2007; Zhang et al., 2019). Recruitment of the GLT Prs to the Eμ:3′Eα loop anchors mediates the synapsis of S regions and initiates GLT expression (Feldman et al., 2015;

Author Manuscript Author Manuscript Author Manuscript Author Manuscript

Pinaud et al., 2001; Wuerffel et al., 2007) and facilitates the targeting of S regions by AID (Pavri et al., 2010; Pefanis et al., 2014; Zheng et al., 2015) (Figures 1A and 1B).

Class switching to downstream isotypes may proceed directly from IgM or via a sequential pathway (Matsuoka et al., 1990). Direct switching to IgE is tightly correlated with Igh locus chromatin conformation in developing B cells (Kumar et al., 2013) and dependent on genomic context (Feldman et al., 2015; Jung et al., 1994; Lorenz et al., 1995; Misaghi et al., 2010). However, switching to IgE through a direct μ→ε approach occurs infrequently in mature B cells (Mandler et al., 1993; Siebenkotten et al., 1992). Although the molecular pathway chosen for downstream isotype switching has physiological implications that may be dependent on Igh locus topology, little is known regarding the overall topological conformation of the Igh locus and its relationship to CSR efficiency and specificity.

Chromosomes contain topologically associated domains (TADs), also termed contact domains, that have been detected using chromosome conformation capture (3C)-based technology (Dekker and Mirny, 2016; Dixon et al., 2012; Lieberman-Aiden et al., 2009; Nora et al., 2012; Rao et al., 2014; Sexton et al., 2012). TADs are frequently anchored by DNA elements bound by the architectural protein CTCF and its partner the SMC cohesin complex (Rao et al., 2014; Rowley and Corces, 2018). The observation that CTCF binding elements (CBEs) situated at TAD boundaries are often in a convergent orientation (Rao et al., 2014) has led to the proposition that chromatin loops are formed by an extrusion mechanism mediated by cohesin (Fudenberg et al., 2016; Nasmyth, 2001; Nichols and Corces, 2015; Sanborn et al., 2015). Hi-C maps have revealed architectural “stripes” (Vian et al., 2018) that may form when one subunit of cohesin stalls near a strong CTCF loop anchor while the second one slides along the chromatin to form a plethora of contacts. A functional relationship between architectural stripes and CSR was revealed when deletion of the CBE cluster at the 3′ boundary of the Igh locus led to loss of the associated chromatin stripe and a reduction of GLT expression and CSR (Vian et al., 2018).

Here, we examine the relationship between developmentally regulated higher-order chromatin structure at the Igh locus, and the order of events leading to isotype switching. Using 3C techniques, we find a strikingly high frequency of chromatin contacts that are asymmetrically anchored at the 3′Igh boundary and distributed among the downstream C_H regions in B cells. To accommodate these observations, we posited an alternative CSR pathway in which downstream 3′Eα tracks along the locus via loop extrusion and facilitates formation of GLT Pr-Pr interactions and downstream S-S synapses. We provide functional evidence of high-frequency CSR between downstream S regions leading to IgE switching and bypassing IgG1 expression. Our studies have combined the strategies of following diagnostic CSR products in phenotypically distinct subsets of B cells have led to identification of a B cell receptor (BCR)-negative B cell intermediate that is pivotal to efficient CSR.

Author Manuscript Author Manuscript Author Manuscript Author Manuscript

RESULTS

Asymmetric loop extrusion implies the directionality of CSR

To better understand Igh locus conformation we interrogated 3′Igh chromatin topology at several stages of B cell development and in T cells using high resolution 4C sequencing (4C-seq) and viewpoints at Eμ and 3′Eα (hs4) (Figure 1A) (van de Werken et al., 2012b). For these studies splenic B cells were activated with lipopolysaccharide (LPS)+interleukin (IL)-4 for 40 h, and CSR is not detected until about 2.5 days post-stimulation (Feldman et al., 2017; Wuerffel et al., 2007). The Eμ viewpoint preferentially interacts with the 3′Eα sites hs4, hs1,2, and hs3a (red intensities) to form a large loop with few contacts in the genomic interval separating these enhancers in Rag-deficient pro-B cells (Figure 1C). Eμ:3′Eα contacts progressively increase in resting and activated B cells and are absent in T cells, consistent with previous studies (Figure 1C) (Feldman et al., 2017; Kumar et al., 2013; Wuerffel et al., 2007). The Eμ interaction with an enhancer located between Cγ1 and Cγ2b regions (Predeus et al., 2014; Whyte et al., 2013), that we term Eγ, is detected in pro-B cells (orange circle) (Figure 1C). Although these interactions are more difficult to detect in mature B cells, they can be found using 5C and 3C assays, as detailed below.

Intra-3′Eα interactions (red intensities) and the Eμ:3′Eα contact profile anchored at hs4 are similar to those found for the Eμ bait (Figure 1D). However, the locus-wide 4C interactions originating from the hs4 viewpoint displayed a distinctly different profile of chromatin contacts than that observed for the Eμ bait (Figure 1D). Frequent hs4 anchored chromatin contacts are observed at multiple sites (blue intensities) including Eγ and Eμ at all B cell stages and are absent in T cells (Figures 1D and 1E). 3′Eα-Eγ interactions (blue intensities) are significantly more frequent than those found for Eμ-Eγ contacts (teal intensities) (Figures 1C and 1D). Accordingly, Eμ preferentially associates with 3′Eα, whereas 3′Eα interacts with both Eμ and with GLT Prs in activated B cells (Feldman et al., 2015; Feldman et al., 2017). The 3′Eα interaction profile has similarities to architectural stripes (Benner et al., 2015) that are thought to form through an extrusion mechanism mediated by one subunit of cohesion stalling near a strong CTCF loop anchor such as that found at the 3′RR while the second one slides along the chromatin to form multiple contacts (Vian et al., 2018) (Figures S1A–S1C). The hs4 4C contact profile could plausibly be generated through asymmetric loop extrusion that initiates at 3′Eα terminates at Eμ, and could explain the relative lack of Eμ contacts within this genomic interval. The plethora of chromatin contacts anchored by 3′Eα may exist independent of the 3′Eα:Eμ loop with implications for the mechanism of CSR (Figure 1E).

High-frequency 3′Eα interactions are developmentally regulated

To further explore Igh locus conformation we examined chromatin contacts at high resolution in 5C libraries from previously reported mouse embryonic fibroblasts (MEFs), $Rag2^{-/-}$ pro-B cells (Montefiori et al., 2016), and in newly derived resting and activated B cells (Figure S2). Difference heatmaps were constructed by subtracting normalized MEF-derived from B cell-derived 5C datasets to identify MEF (blue intensities) and B cell (red intensities) prevalent interactions (Figure 1F). The 3′Igh TAD boundary is evident in MEFs and at all stages of B cell development (green arrows) (Figure 1F). Intra-3′Eα chromatin

Author Manuscript Author Manuscript Author Manuscript Author Manuscript

contacts (yellow box) are enriched in Rag2$^{-/-}$ pro-B cells as compared to MEFs and are further increased in resting and activated splenic B cells, consistent with our 4C findings and the progressive developmental activation of this enhancer (Garrett et al., 2005) (Figure 1F). The 5C difference maps also indicate the presence of Eμ:3′Eα (black ovals) interactions at all stages of B cell development relative to MEFs, in agreement with our earlier studies (Figure 1F) (Feldman et al., 2017; Kumar et al., 2013; Wuerffel et al., 2007). Eγ interacts with Eμ (blue ovals) and 3′Eα (yellow ovals) at all B cell developmental stages (Figure 1F). Eγ also associates with γ3 to form loops spanning γ2b, γ2a, ε and α C_H genes (teal box), and the γ1–γ3 C_H genes (blue box), raising the possibility that Eγ anchors a secondary loop that could provide proximity of the downstream GLT Prs with 3′Eα and to each other (Figure 1F). The frequency of chromatin contacts within these loops progressively increase as the cells transition from pro-B to activated B cells (Figure 1F). Frequent 5C contacts spanning the 3′Eα-Eμ genomic interval are similar to the 4C-seq contact pattern from the hs4 viewpoint and provide evidence for a 3′Eα-Eγ loop that structures the Igh locus throughout B cell development.

Using 3C assays we showed that γ3-γ1 interactions increased significantly in LPS+IL-4-activated B cells and are only minimally increased following LPS treatment relative to resting B cells (Figure S3A). LPS+IL-4 activation conditions favor γ1 and repress but do not extinguish γ3 GLT expression (see Figure 2D), making it possible for the γ1–γ3 GLT Prs to interact under these conditions. Furthermore, we confirmed the presence of frequent 3′Eα:Eγ contacts that could facilitate formation of 3′Eα:Eγ:GLT Pr loops following B cell activation. Intra-3′Eα looping between 3C anchor hs3b,4 (fragment H) and hs3a (fragment F) are induced in both activated B cells relative to resting B cells, validating the integrity of the chromatin samples (Feldman et al., 2015; Feldman et al., 2017) (Figure S3B). GLT Prs are differentially activated to associate with hs3b,4 (fragment H) (Feldman et al., 2015; Wuerffel et al., 2007). Accordingly, hs3b,4:γ2b (H:D) and γ2b:hs3b,4 (D:H) looping interactions are elevated in LPS-activated B cells, whereas hs3b,4:γ1 (H:C) contacts are highly induced following LPS+IL-4 treatment (Figure S3B). Eγ and the γ1 GLT Prs are located on a single 20-kb HindIII fragment (C) and can be separated following HindIII and EcoRI digestion to generate the γ1 GLT Pr (Ca) and Eγ (Cb) fragments (Figure S3B, top panel). Hs3b,4:γ1 (H:Ca, H:C) contacts are elevated in LPS+IL-4 as compared to LPS-activated or resting B cells (Figure S3B; Figure 1G) (Feldman et al., 2015). In contrast, both activation conditions lead to increased frequency of hs3b,4:Eγ interactions (H:Cb and H:C fragments), confirming that 3′Eα:Eγ looping occurs in activated B cells.

An alternate pathway for IgE switching

To explore the involvement of downstream S-S synapsis in CSR, we consider the case of IgE switching that is thought to occur through a sequential CSR pathway and rarely via direct switching (Mandler et al., 1993; Siebenkotten et al., 1992; Yoshida et al., 1990) (Figures 2A and 2B). During direct switching, Sμ-Sε hybrid junctions are formed with the concomitant deletion of the intervening genomic material (Figure 2A). Sequential switching initiates with recombination between Sμ and Sγ1 to form hybrid SμSγ1, leading to expression of IgG1, and next recombines with Sε to generate the SμSγ1Sε and produce IgE (Yoshida et al., 1990) (Figure 2B). A third pathway involves recombination between downstream

Author Manuscript Author Manuscript Author Manuscript Author Manuscript

Sγ1 and Sε, retention of surface IgM^+ followed by Sμ recombination with Sγ1Sε, and a switch to IgE without generating $IgG1^+$ B cells (Figure 2C). We term this reverse sequential switching since it initiates with recombination between downstream isotypes and ends with recombination at Sμ. CSR pathways can be monitored by the expression of distinct transcripts, including GLTs, post-switch transcripts (PSTs), downstream PSTs (dPSTs), and circle transcripts (CTs), in response to distinct CSR activation protocols (Figure S4). dPSTs involving an I exon and a C_H gene are expressed when two downstream S regions recombine and are uniquely diagnostic of the reverse sequential CSR pathway (Figure 2C; Figure S4).

Reverse sequential switching occurs in activated B cells

To assess the use of the reverse sequential pathway in CSR, B cells were stimulated with four activation protocols to induce different combinations of secondary isotypes (Figure S4B). We used homozygous M1 prime GFP knockin mice to detect B cells that express the ε GLT as well as those that have switched to IgE (Talay et al., 2012). Surface IgE cannot be directly assessed because the Fc receptor for IgE (CD23) is expressed on activated B cells and binds soluble IgE to non-IgE-expressing B cells (Conrad et al., 1988). Consequently, we analyzed the frequency of surface IgM, IgG1, cytoplasmic IgE, and GFP expression in activated B cells. LPS-activated B cells switch only to IgG3 and IgG2b and fail to express GFP (Figure S5A). Stimulation with anti-δ-dex+LPS+IL-4+IL-5+Blys+transforming growth factor (TGF)-β (αδ-dex cocktail) induces switching to IgG2b, IgG1, IgE, and IgA (Kaminski and Stavnezer, 2007; McIntyre et al., 1995) and GFP expression. We show that the αδ-dex cocktail without TGF-β (NOT) promotes expression of GFP and switching to IgG1 and IgE as does stimulation with LPS+IL-4 (Figures S5A and S5B).

The GLT expression profile for each induction condition is well correlated with the PST and dPST expression patterns (Figure 2D). The α-δ-dex cocktail induces expression of γ2b, γ1, ε and α GLTs, and related PSTs (Figure 2D). The strikingly robust levels of dPSTs Iγ1Cγ2b, Iγ1Cε, Iγ1Cα, and Iγ2bCα increase from day 3 to day 4 of stimulation, indicating that that these intermediates are a feature of CSR (Figure 2D). The GLTs γ1 and ε and PSTs IμCγ1 and IμCε are detected following B cell activation with NOT and LPS+IL-4, indicating more limited switching to IgG1 and IgE (Figure 2D). Likewise, GLTs γ3 and γ2b and PSTs IμCγ3 and IμCγ2b were induced upon LPS treatment (Figure 2D). Downstream PSTs are restricted to Iγ1Cε in response to NOT and LPS+IL-4, and to Iγ3Cγ2b upon LPS induction, demonstrating a strict correlation of dPST and GLT expression. LPS-induced Iγ3Cγ2b dPSTs are not expressed in $AID^{-/-}$ B cells, indicating a strict dependency on CSR for their expression (Figure S6C).

CT expression verifies that dPSTs originate from dynamic CSR events (Matsuoka et al., 1990; Yoshida et al., 1990) (Figure 2A). CTs Iγ3Cμ and Iγ2bCμ are present in LPS-activated B cells, indicating that direct IgG3 and IgG2b switching occurs (Figure 2E). The α-δ-dex cocktail-induced CTs Iγ1Cμ, Iγ2bCμ, and IαCμ are correlated with the GLT and PST expression profiles and are indicators of direct switching (Figure 2E). Notably, the IεCμ CT was undetectable in B cells activated with the α-δ-dex cocktail or with LPS+IL-4 (Figure 2E). Detection of IεCμ CT (*IεCμ) required 4-fold higher input of cDNA than for all other CT amplification reactions, indicating that direct switching from IgM to IgE

Author Manuscript Author Manuscript Author Manuscript Author Manuscript

occurs infrequently (Figures 2B and 2C), as previously observed (Mandler et al., 1993; Siebenkotten et al., 1992). The CT intermediates of sequential switching, IεCγ1 and IαCγ1, are also found (Figure 2E). The generation of isotype-specific dPSTs in response to defined B cell induction protocols and the absence of direct IgE switching imply that the reverse sequential switching pathway is functional.

B cells transitionally express IgM^+IgG1^+ followed by $IgG1^+$, $IgG1^+IgE^+$, and finally IgE^+ during the course of sequential IgE switching. The reverse sequential IgE switching model predicts expression of only IgM^+IgE^+ B cells (Figure 2C). To test this proposition, B cells were activated with NOT for 40 h, 3 days, and 4 days and $IgG1^-$ and $IgG1^+$ cells were gated and then further analyzed for IgM and IgE expression (Figure 2F). Active switching from IgM to IgG1 was the dominant event as reflected in the presence of IgM^+IgG1^+ B cells (white stack) (Figure 2G). Detection of $IgM^+IgG1^+IgE^+$ (orange stack) and $IgM^-IgG1^+IgE^+$ B cells (red stack) on day 3 of stimulation is a direct reflection of sequential IgE switching (Figure 2G). IgM^+IgE^+ B cells (blue stack) are enriched on day 3 and diminished on day 4 of stimulation, consistent with active reverse sequential switching at early time points (Figure 2G). The presence of $IgM^-IgG1^+IgE^+$ and IgM^+IgE^+ B cells indicates the co-existence of the sequential and reverse sequential switching pathways.

Downstream PSTs are generated on the productively rearranged Igh allele

To deduce whether downstream switching is associated with the productively rearranged allele, we used heterozygous tdTomato (tdTom) mice in which the Iε-tdTom Igh allele was inactivated for IgE switching (Figure 3A) (Wu et al., 2017). C57BL/6 × BALB/$c^{Iε\text{-}tdTom}$ F_1 B cells carrying Igh loci of the b and a allotypes, respectively, were pre-sorted for IgM^b and IgM^a B cells and activated with NOT for 3 and 4 days (Figure 3B). This approach allowed us to follow the productively rearranged allele that is either permissive (Ig^b) or blocked (Ig^a) for IgE switching (Figure 3B). Activated cultures initially expressing IgM^a or IgM^b each contained $IgG1^-$ and $IgG1^+$ B cells that were further analyzed for IgM and IgE (Figure 3C). The $IgG1^+$ switching frequency was similar in both IgM^a and IgM^b cell-seeded cultures and increased from day 3 to day 4 (Figures 3C and 3D). All IgE-related switching is greatly diminished in cultures seeded with IgM^a cells, consistent with the block to IgE switching on the tdTom allele (Figures 3C and 3D). In contrast, IgE^+ switched B cells are clearly detected in cultures initiated with IgM^b cells, and the presence of $IgM^+IgG1^+IgE^+$ (orange stack) and $IgG1^+IgE^+$ (red stack) cells indicates that sequential switching is active (Figures 3C and 3D). The proportions of IgM^+IgG1^+ (white stack), $IgM^+IgG1^+IgE^+$, and $IgG1^+IgE^+$ B cells increase at day 4 compared to day 3, implying that the sequential switching pathway may be fed forward by the increase of IgM^+IgG1^+ B cells on day 3.

IgM^+IgE^+ (blue stack) B cells, associated with the reverse sequential pathway, are enriched at both day 3 and day 4 of stimulation in cultures initiated with IgM^b B cells and are substantially reduced in cultures seeded with IgM^a B cells (Figures 3C and 3D). The relative absence of $IgM^+IgG1^+IgE^+$ and $IgG1^+IgE^+$ B cells until day 4 suggests that the reverse sequential pathway may dominate at early time points. The very low but still detectable levels of IgM^+IgE^+ B cells in IgM^a-seeded cultures may arise from low level trans-IgE switching between the Ig^b and Ig^a alleles to side-step the blocked tdTom allele as noted

Author Manuscript Author Manuscript Author Manuscript Author Manuscript

in rabbit and mouse B cells (Figures 3C and 3D) (Dougier et al., 2006; Kingzette et al., 1998; Reynaud et al., 2005). It is formally possible that IgG1 was once expressed and is now extinguished in IgM^+IgE^+ B cells. However, it is unclear how IgG1 could be specifically lost while both IgM^+IgE^+ remain on the B cell surface.

To assess diagnostic transcripts associated with direct or reverse sequential switching, we analyzed expression of PSTs, CTs, and V_HC_H MTs in IgM^a- and IgM^b-seeded cultures (Figure 3E). MTs for $V_HC\mu$, $V_HC\gamma1$ and PSTs $I\mu C\gamma1$ are present in both culture types, indicating that IgM transcription and IgG1 switching occur successfully on both Ig alleles (Figure 3E). In contrast, $V_HC\varepsilon$ MTs are expressed only in IgM^b-derived and not in IgM^a-derived B cells (Figure 3E). Importantly, $I\gamma1C\varepsilon$ dPSTs are expressed in IgM^b-seeded cultures, indicating that step 1 of reverse sequential recombination has occurred on the productively rearranged allele that supports IgE switching (Figure 3E). $I\gamma1C\varepsilon$ dPSTs that originate from the nonproductively rearranged Ig^b allele do not contribute to IgE expression in IgM^a-derived B cells (Figures 3B and 3E). Finally, expression of $I\gamma1C\mu$ and $I\varepsilon C\gamma1$ CTs is found in both IgM^a and IgM^b seeded cultures, indicating that CSR is a dynamic process (Figure 3E). $I\varepsilon C\mu$ CTs are undetectable in both IgM^a- and IgM^b-derived B cells, confirming that direct switching is extremely rare on the Ig^b allele (Figure 3E). The emergence of IgM^+IgE^+ B cells in conjunction with expression of $I\gamma1C\varepsilon$ dPSTs from the Ig^b productive allele and the absence $I\varepsilon C\mu$ CTs are evidence that a portion of IgE switching occurs via the reverse sequential pathway.

Reverse sequential IgE switching is dominant in B cells from BALB/c mice

To determine whether the reverse sequential pathway is a general feature of CSR in the wild-type (WT) context, we tracked expressed Ig phenotypes in NOT activated B cells from C57BL/6 and BALB/c mice. Flow cytometry analyses indicate that the $IgG1^+$ switching frequency (gray stack) was elevated in B cells from C57BL/6 as compared to BALB/c mice and increased from day 3 to day 4 of stimulation in quantitative analyses (Figures 4A and 4B). Although IgE^+-switched B cells (black stack) are more prominent in C57BL/6 cultures, they are still detected in B cells from BALB/c mice (Figure 4B). The proportion of IgM^+IgG1^+ (white stack), $IgM^+IgG1^+IgE^+$ (orange stack), and $IgG1^+IgE^+$ (red stack) B cells increased at day 4 compared to day 3 in C57BL/6-derived B cells, indicating that the sequential switching pathway is active and may be fed forward by IgM^+IgG1^+ B cells on day 3, a pattern observed for B cells from M1 primer GFP^+ mice (Figures 2G and 4B). In contrast, $IgM^+IgG1^+IgE^+$ and $IgG1^+IgE^+$ cells are rare in BALB/c-derived B cells, indicating that sequential switching is infrequent and the reverse sequential pathway is dominant for IgE switching in BALB/c-derived B cells (Figure 4B). Direct switching is extremely rare in both BALB/c- and C57BL/6-derived B cells, as $I\varepsilon C\mu$ CTs are undetectable whereas $I\gamma1C\mu$ CT expression is evident (Figure 5C). The low level of $I\varepsilon C\gamma1$ CT expression level in BALB/c as compared to C57BL/6 B cells may reflect overall lower frequency CSR.

We extended the analysis of CSR pathways to IgG3/IgG2b switching in LPS-activated B cells from C57BL/6 and BALB/c mice. Switching to IgG3 occurs through direct CSR, whereas IgG2b switching can potentially occur through all three pathways (Figures 2A–2C). We found that direct and reverse sequential pathways dominate for IgG2b switching

Author Manuscript Author Manuscript Author Manuscript Author Manuscript

in both C57BL/6- and BALB/c-derived B cells, an interpretation supported by Ig surface phenotype and the expression of the Iγ3Cγ2b dPST and Iγ2bCμ CTs (Figure S6A–S6C). Importantly, CSR-dependent transcripts were absent in $AID^{-/-}$ B cells, further verifying their authenticity (Figures S6C and S6D). Ig surface isotype analyses indicated that although $IgG2b^+$ B cells (black stack) were detected, only modest numbers of $IgM^+IgG3^+IgG2b^+$ (orange stack) and $IgM^-IgG3^+IgG2b^+$ (red stack) B cells were present, indicating that IgG2b sequential switching is not frequently used in both mouse genotypes (Figure S6B). In contrast, $IgM^+IgG3^-IgG2b^+$ (blue stack) B cells were found at robust frequencies that accrue in C57BL/6-derived but not in BALB/c-derived B cells, suggesting that the direct and/or reverse sequential pathways are preferred for IgG2b switching (Figure S6B). Lower PSTs IμCγ3 and IμCγ2b expression levels for BALB/c-derived B cells are consistent with lower frequencies of IgG3 and IgG2b switching relative to that from C57BL/6 (Figure S6C). Expression of the Iγ3Cγ2b dPST, diagnostic for step 1 of reverse sequential IgG2b switching, was elevated in both the C57BL/6 and BALB/c genotypes and absent in $AID^{-/-}$ B cells where CSR is abolished, indicating that the reverse sequential pathway is operational in both strains of mice (Figure S6C). Detection of the Iγ2bCμ CT indicates that the direct IgG2b switching pathway functions in conjunction with the reverse sequential pathway in C57BL/6 B cells (Figure S6C). The relative absence of the Iγ2bCμ CT in BALB/c B cells indicates that the reverse sequential pathway is the primary conduit for IgG2b switching in this mouse strain.

Collectively, our data indicate that γ3, γ2b, and γ1 loci undergo direct CSR and that direct and reverse sequential CSR pathways account for most IgG2b switching. In contrast, IgE CSR occurs via the sequential and reverse sequential pathways. Use of the IgE sequential pathway was strain specific and preferentially occurred in C57BL/6-derived B cells. Thus, reverse sequential CSR may be a common pathway for IgE switching in various strains of mice. Previous studies concluded that B cells engage in direct and sequential IgE switching pathways based on the sequence of composite S/S regions (He et al., 2013; Xiong et al., 2012). However, the Sμ/Sε signature, produced by direct CSR, may also form during sequential switching upon deletion of the Sγ1 remnant. The Sμ/Sγ1/Sε hybrid is generated following both reverse and sequential switching, making it difficult to distinguish these pathways (Figures 2B and 2C). Thus, our findings need not be discrepant with earlier findings.

IgM^-IgG^- B cells harbor downstream PSTs

Using B cells from homozygous M1 prime GFP knockin ($M1'GFP^+$) mice we asked whether Iγ1Cε dPSTs are enriched in GFP^+ B cells that are potentiated for IgE switching. GFP expression allows detection of B cells that express the ε GLT as well as those that have switched to IgE (Talay et al., 2012). NOT activated B cells reproducibly display heterogeneous levels of IgM expression ranging from IgM^+ to IgM^- on day 4 of stimulation (Figure 5A). Activated B cells gated for high IgM fluorescence rarely co-express IgG1 or IgE, whereas IgM^- B cells are enriched for switched isotypes (Figure 5A, right panels). Therefore, IgM^+ (bound) and IgM^- (flowthrough) subpopulations were isolated and further purified based on GFP and IgG1 expression and then assessed for expression of CSR-related transcripts (Figures 5B and 5C). In parallel, we analyzed each B cell subset for cytoplasmic

Author Manuscript Author Manuscript Author Manuscript Author Manuscript

IgE expression by flow cytometry (Figure 5D). AID transcripts are expressed in most cell subsets (Figure 5C). IμCγ1 PST expression is elevated in $IgG1^+$ cells (columns 2, 4, 6, and 8) and decreased in $IgG1^-$ cells (columns 1, 3, 5, and 7) for both IgM^+ and IgM^- subgroups, indicating the tight correlation between Ig surface phenotype and PST expression (Figure 5C). Indeed, highly abundant $IgM^+GFP^-IgG1^-IgE^-$ cells fail to express AID transcripts, PSTs, and dPSTs, indicating the diminished potential for CSR (Figures 5C and 6D, column 3). Two categories of B cells were of particular interest. First, small fractions of the $IgM^+GFP^+IgG1^+$ and $IgM^-GFP^+IgG1^+$ subsets are IgE^+, are switching through the sequential pathway, and, accordingly, express low levels of IμCε PSTs and Iγ1Cε dPSTs (Figure 6D, columns 2 and 6). Second, the abundant $IgM^-GFP^+IgG1^-$ subset is enriched in IgE^+ B cells (>20%) and expresses high levels of IμCε PSTs and Iγ1Cε dPST with concomitant low levels of IμCγ1 PST, indicating that these cells have undergone or are actively engaged in IgE switching (Figures 5C and 5D, column 5). IεCγ1 CTs are found in all three of these GFP^+ B cell subgroups, indicating that IgE switching is actively occurring (Figure 5C, columns 2, 5, and 6). Thus, Iγ1Cε dPST expression is strongly associated with cells that have undergone or are actively engaged in IgE switching.

To further explore the possibility that dPSTs occur in B cells potentiated for reverse sequential switching, we examined surface $IgG3^+$ and $IgG2b^+$ B cells that preferentially emerge from the IgM^- B cell subset following LPS activation (Figure 5E). IgM^- B cells were separated into $IgG3^+$, $IgG2b^+$, and $IgG3^-IgG2b^-$ subsets and assessed for CSR-related transcripts (Figures 5F and 5G). AID transcripts were enriched in all three B cell subsets and were highest for triple negative (TN) $IgM^-IgG3^-IgG2b^-$ B cells, suggesting that these cells are potentiated for CSR relative to unfractionated cells (Figure 5G, column 2). High levels of IμCγ3 and IμCγ2b PSTs, reporters of CSR, are expressed in $IgG3^+$ and $IgG2b^+$ cells, respectively (Figure 5G, columns 1 and 3). Intriguingly, the Iγ3Cγ2b dPST was highly enriched in TN B cells and was absent in $IgG3^+$ cells, indicating that at least some TN cells have undergone step 1 of the reverse sequential switching and may be cellular intermediates in CSR (Figure 5G, column 2).

Switching B cells dynamically cycle through a BCR^{neg} state

To test the proposition that LPS-activated TN B cells are intermediates in isotype switching, IgM^+ (bound) and IgM^-/IgM^{dim} (flowthrough) subgroups were column purified and further fluorescence-activated cell sorting (FACS) purified (Figure 6A). The frequency of $IgG3^+$ and $IgG2b^+$ cells was reproducibly highest for the IgM^- subpopulation, diminished for the IgM^{dim} subpopulation, and negligible for the IgM^+ subpopulations (Figure 6A, left panels). Re-culture of purified $IgM^+IgG3^-IgG2b^-$, $IgM^{dim}IgG3^-$ $IgG2b^-$, and TN $IgM^-IgG3^-IgG2b^-$ cells in LPS for 24 h led to the dynamic re-expression of heterogeneous levels of IgM in all cases (Figure 6A, i–iii, orange arrows). Essentially, all $IgG3^+$ and $IgG2b^+$ B cells emerged from IgM^- cells and not from IgM^+ cells following re-culture (Figure 6A, rightmost panels). Our observations that activated B cells dynamically transition between IgM^+ and TN states and that the TN state has the highest capacity to isotype switch suggest that TN cells engage in CSR (Figures 5G and 6A).

Author Manuscript Author Manuscript Author Manuscript Author Manuscript

To test the notion that TN cells are highly potentiated for CSR, IgM^- cells were divided into two subsets, $IgM^-IgD^-IgG3^-$ $IgG2b^-Ig\kappa^-$ (BCR^{neg}) (orange) and $IgM^-IgD^+IgG3^-IgG2b^-Ig\kappa^+$ ($IgD^+Ig\kappa^+$) (blue) (Figure 6B). BCR^{neg} and $IgD^+Ig\kappa^+$ cells were re-cultured in LPS for 24 h and analyzed for IgM expression and engagement in CSR. BCR^{neg} but not $IgD^+Ig\kappa^+$ cells regenerated a heterogeneous population of IgM^+ and IgM^- B cells and supported switching to IgG3 and IgG2b (Figure 6B, I and ii). The re-culture system confirms the dynamic transition between the IgM^+ and BCR^{neg} states and the capacity of BCR^{neg} cells to undergo CSR (Figure 6C).

Transcriptional silencing of the Igμ locus in BCR^{neg} B cells

B cells undergoing CSR are in G_1 of the cell cycle (Schrader et al., 2007) and have experienced at least five cell divisions (Hodgkin et al., 1996). To better characterize BCR^{neg} cells, LPS-activated $IgM^{dim}IgD^-CD138^-$ (brown) and $IgM^-IgD^-IgG3^-IgG2b^-Ig\kappa^-Ig\lambda^-CD138^-$ ($BCR^{neg}CD138^-$; orange) B cells were gated to exclude $CD138^+$ plasma cells and were then assessed for cell cycle and proliferation history (Figure 7A). $BCR^{neg}CD138^-$ cells are almost exclusively in the G_1 phase when analyzed with Vybrant DyeCycle (Figure 7B). In contrast, $IgM^{dim}IgD^-CD138^-$ B cells are found in all cell cycle phases, indicating that these cells are actively proliferating (Figure 7B). Carboxyfluorescein succinimidyl ester (CFSE) labeling of B cells to assess cumulative cell divisions shows that most $BCR^{neg}CD138^-$ and $IgM^{dim}IgD^-$ $CD138^-$ B cells had experienced more than five cell divisions, indicating that $BCR^{neg}CD138^-$ B cells had a normal proliferative history (Figure S7). We conclude that $BCR^{neg}CD138^-$ cells reside in the G_1 cell cycle phase and are capable of dynamic proliferation and re-expression of IgM as demonstrated in re-culture studies (Figures 6A, iii, and 6B, i).

Emergence of surface BCR^{neg} B cells led us to examine the status of intra-cellular Ig protein expression in $BCR^{neg}CD138^-$ and $IgM^{dim}IgD^-CD138^-$ B cells (Figure 7A). Using fluorescence microscopy we found that both $BCR^{neg}CD138^-$ and IgM^{dim} IgD^-CD138^- B cells exhibit B220 on the membrane surface and were essentially negative for IgG (IgG3/IgG2b) (Figure 7C). Cytoplasmic IgM was detected in $IgM^{dim}IgD^-CD138^-$ as expected from their surface IgM profile but not in $BCR^{neg}CD138^-$ B cells (Figure 7C). Igμ expression is blocked at the transcriptional level in $BCR^{neg}CD138^-$ cells since VHJ558Cμ MTs and IμCμ GLTs are largely abolished as compared to unfractionated controls (Figure 7D). In contrast, the expression of AID, the Iγ3Cμ, Iγ2bCμ GLTs, and CD79a and CD79b co-receptor transcripts is similar in both groups (Figure 7D). Thus, Igμ mRNA expression is lost in BCR^{neg} B cells whereas other Igh- and BCR-related transcripts are expressed at normal levels. A transcriptionally silenced Igμ locus cannot be targeted by AID and would favor redirection of AID attack to transcriptionally active downstream S regions and promote step 1 of the reverse sequential switching pathway.

Emergence of BCR^{neg} cells is linked to AID-induced DNA damage

To investigate whether the emergence of $BCR^{neg}CD138^-$ B cells is linked to the mechanism of CSR we examined LPS-activated B cells from WT, $AID^{-/-}$, and $53BP1^{-/-}$ B cells using a sequential FACS gating strategy (Figure 7E). AID deaminates dC residues, thereby initiating a cascade of events leading to DNA DSBs in transcribed S regions (Kenter, 2012; Schrader

Author Manuscript Author Manuscript Author Manuscript Author Manuscript

et al., 2007; Wuerffel et al., 1997). In the absence of 53BP1 AID induced the DSBs persist but recombination is severely impaired (Dong et al., 2015; Feldman et al., 2017; Khair et al., 2014; Manis et al., 2004). We find that the frequency of $CD138^{-}BCR^{neg}$ B cells is dependent on AID-induced DNA damage since the number of these cells is significantly reduced in the absence of AID (0.5%) as compared to WT (2%) and significantly increased when DSBs accumulate in $53BP1^{-/-}$ B cells (6%) (Figures 7E and 7F). Hence, the elevated frequency of $BCR^{neg}CD138^{-}$ B cells following LPS induction appears to be dependent on induction and persistence of AID-instigated DSBs.

DISCUSSION

In this study, we have shown that Igh chromatin loops most likely formed by loop extrusion promote downstream GLT-Pr-E interactions and predict an alternative pathway for isotype switching. Our chromatin conformation capture-based studies revealed that although Eμ almost exclusively associates with 3′Eα in a point-to-point anchored loop, the 3′Eα interaction pattern is multifocal and reminiscent of architectural stripes (Benner et al., 2015), the formation of which has been attributed to chromatin loop extrusion (Vian et al., 2018). Our demonstration that 3′Eα associates with Eγ and provides an anchor that tethers downstream GLT Prs also creates spatial proximity between their paired S regions and facilitates downstream CSR with no attendant change of surface Ig isotype. Recognition that downstream CSR might be followed by recombination with Sμ provided a rubric for the reverse sequential switching pathway. This pathway is consequential, as it may permit rapid progression from IgM^{+} to distant downstream secondary isotypes in response to pathogens. Indeed, IgM^{+} memory cells that had experienced γ1→ε CSR could undergo a subsequent switch to IgE expression via the reverse sequential pathway.

Several lines of evidence confirm key elements of the reverse sequential switching model and have in addition identified a BCR^{neg} B cell intermediate in this pathway. The robust expression of correlated GLTs, PSTs, and dPSTs with several B cell activation protocols provides functional evidence of GLT Pr-Pr-3′Eα proximity in chromatin. We confirmed that direct μ→ε switching is very rare (Mandler et al., 1993; Siebenkotten et al., 1992) and detected expression of diagnostic Iγ1Cε dPSTs associated with step 1 of IgE reverse sequential switching. Using mice in which the ε locus was inactivated on one allele, we demonstrated that reverse sequential switching can occur on the productively rearranged allele and contribute to IgE expression. Although the sequential and reverse sequential pathways are active in B cells from C57BL/6 mice, only reverse sequential switching is active in the BALB/c context and appears to be the primary source for IgE. Finally, IgG2b switching appears to be mediated through a combination of direct and reverse sequential switching, indicating that the reverse sequential pathways is broadly used. Taken together, our findings challenge the wide-spread idea that switching is unidirectional and initiates from upstream Sμ.

The assumption of strict directionality in isotype switching from upstream donor Sμ to downstream S regions is based on several interrelated observations. Switching from IgM to downstream secondary isotypes follows the natural polarity of C_H region genes along the locus. Furthermore, AID-induced mutations (Nagaoka et al., 2002; Petersen et al., 2001;

Author Manuscript Author Manuscript Author Manuscript Author Manuscript

Schrader et al., 2003; Xue et al., 2006) and internal deletions (Dudley et al., 2002; Reina-San-Martin et al., 2007) are preferentially targeted to Sμ as compared to downstream S regions, implying that Sμ drives the process of recombination. Therefore, it was unclear how AID targeting is re-directed to downstream S regions during reverse sequential switching in the WT context. We found that activated B cells induced to undergo CSR become BCR^{neg} and in which the Igμ locus was transcriptionally silent. When Sμ transcription is suppressed (Gu et al., 1993) or Sμ is deleted (Zhang et al., 2010), then downstream S regions are a substrate for AID. Accordingly, BCR^{neg} B cells are strikingly enriched for diagnostic dPSTs, indicating that downstream S regions have been targeted by AID and could progress to step 2 of the reverse sequential pathway. Transcriptional silencing of the Igμ locus provides a means by which AID can be preferentially targeted to downstream S regions. However, it was unclear how μ locus transcription is silenced in BCR^{neg} cells.

Cells respond to DNA DSBs by repressing transcription in flanking chromatin in an ATM-dependent fashion (Iannelli et al., 2017; Shanbhag et al., 2010; Ui et al., 2015). We propose that AID-induced DNA lesions at Sμ trigger local transcription inhibition that in turn silences BCR expression. The Sμ region is the most intensively AID-targeted template in the Igh locus (Schrader et al., 2003; Xue et al., 2006) and therefore potentially most prone to transcription repression. The BCR^{neg} condition may continue until the DNA lesions are repaired or CSR is completed, whereupon surface Ig is re-expressed. Why is transcriptional silencing not observed for downstream C_H regions that are targeted by AID? AID-instigated DSBs occur infrequently in downstream S regions (Schrader et al., 2003; Xue et al., 2006), and transcription repression may be below the level of detection in our assays. We favor the view that AID-dependent DNA lesions at Igμ are the proximate cause for emergence of BCR^{neg} cells, as the frequency of these cells is diminished in the absence of AID and significantly expanded in $53BP1^{-/-}$ B cells where DSBs persist (Dong et al., 2015; Feldman et al., 2017; Khair et al., 2014; Manis et al., 2004).

BCR^{neg} cells reside in G_1 of the cell cycle. Consistently, AID activity (Le and Maizels, 2015; Wang et al., 2017) and AID-dependent DSBs in S regions (Khair et al., 2014) are associated with the G_1 phase in switching B cells. The convergence of these observations implies that the presence of DSBs influences residence in the G_1 phase. Indeed, the absence of BCR-dependent signals may inhibit transitioning between cell cycle phases (Otipoby et al., 2015). It is provocative to consider that AID-induced DNA damage activates a G_1 checkpoint during which DNA DSBs are repaired or consumed in the CSR reaction. The relationship of DNA damage signaling to BCR degradation, μ locus transcriptional silencing, and G1 residence requires further clarification.

Limitations of the study

There are two general B cell activation strategies available for CSR induction in *ex vivo* cultures: (1) stimulation through the Toll-like receptor (TLR)4 receptor using LPS alone or in combination with an anti-IgD reagent (αδdex), and (2) reagents that engage the CD40 receptor and mimic T cell-dependent B cell activation and both require the addition of specific cytokines. Our studies used several LPS/TLR4-based activation conditions to examine CSR pathways. Although CSR was robust as measured by emergence $IgG1^+$ B

Author Manuscript Author Manuscript Author Manuscript Author Manuscript

cells, the frequency of IgE switching was relatively low, and both are commensurate with previous studies (Pone et al., 2012). Importantly, the incidence of IgG1/IgE switching is similar when B cells are activated using reagents that signal through the TLR4 or CD40 receptors (Pone et al., 2012). Going forward it will be interesting to determine whether a CSR activation protocol influences the induction of specific CSR pathways. CSR induction was overall lower in BALB/c-derived as compared to C57BL/6-derived B cells, and this difference may reduce IgE switching to the point where the readouts of sequential versus reverse sequential switching are less reliable. Nevertheless, the frequency of IgM^+IgE^+ B cells was comparable in BALB/c- and C57BL/6-derived B cells, suggesting that the reverse sequential pathway was operational. This is an important question, as *in vivo* studies concluded that B cells from BALB/c mice engage in IgE switching via the direct and sequential pathways using isolated $IgG1^+$ B cells (He et al., 2013; Xiong et al., 2012). However, these studies were not designed to determine the frequency of IgM^+IgE^+ B cells that are intermediates of the reverse sequential CSR pathway and were performed under conditions in which CSR frequency is inherently difficult to determine. Future studies must address whether the CSR pathways detected in *ex vivo* cultures directly map onto isotype switching in physiological settings.

STAR★METHODS

RESOURCE AVAILABILITY

Lead contact—Further information and requests for resources and reagents should be directed to and will be fulfilled by Lead Contact, Amy Kenter (star1@uic.edu).

Materials availability—This study did not generate new unique reagents.

Data and code availability

- 4C and 5C datasets have been deposited at GEO and are publicly available as of the date of publication. Accession numbers are listed in the key resources table. Microscopy data reported in this paper will be shared by the lead contact upon request.
- This paper does not report original code.
- Any addition information to reanalyze the data reported in this paper is available from the lead contact upon request.

EXPERIMENTAL MODEL AND SUBJECT DETAILS

C57BL/6 and BALB/c mice were purchased from Jackson Laboratories. $53BP1^{-/-}$ mice, a gift from Dr. S. Franco (Johns Hopkins), $AID^{-/-}$ mice (Muramatsu et al., 2000), a gift from Dr. T. Honjo (Kyoto University), M1 prime GFP^+ knockin mice (Talay et al., 2012), a gift from Dr. L. Wu (Genentech) were bred at the University of Illinois College of Medicine. Iε-tdTom mice were bred in house at Loyola University Chicago Stritch School of Medicine (Wu et al., 2017). All mice were on the C57BL/6 background except for Iε-tdTom mice which were C57BL/6 × BALB/c F1. All splenic B cell cultures were from mice 8–12 weeks of age. All studies were performed with 3–8 mice to generate at least three

Author Manuscript Author Manuscript Author Manuscript Author Manuscript

independent B cell cultures. All procedures involving mice, their maintenance and breeding were approved by the Institutional Animal Care Committees of the University of Illinois College of Medicine and Loyola University Chicago Stritch School of Medicine. No gender differences were found in these studies thus males and females were used indiscriminately.

Primary B cell cultures were derived from spleens. Splenic B cells were sorted for CD43− resting B cells using anti-CD43 magnetic microbeads (MACS, Miltenyi) according to the manufacturer's instructions. B cells cultured at a density of 5–8 × 10^5 cells/ml in RPMI, glutamine (4 μM), penicillin (100 U/ml)-streptomycin (100 μg/ml), β−mercaptoenthanol (50 μM), supplemented with FCS (20% vol/vol) with the activators, LPS (50 μg/ml), LPS and IL4 (10 ng/ml), the αδ-dex cocktail including αδdex (3 ng/ml), LPS (50 μg/ml), IL4 (10 ng/ml), IL5 (1.5 ng/ml), TGFβ (2 ng/ml), Blys (100 ng/ml) (Kaminski and Stavnezer, 2007), and αδ-dex cocktail in the absence of TGFβ (NOT), or with RP105 (0.65 μg/ml, BD PharMingen). B cells were activated with NOT or LPS for 40 hours, 3- and 4 days and then IgM^+ (bound) and IgM^{dim}/IgM^- (flowthrough) B cells were isolated using anti-IgM magnetic microbeads (MACS, Miltenyi) according to the manufacturer's instructions. Splenic T cells that were enriched using the mouse T cell enrichment column kit (MTCC-5, R&D) and cultured with ConA (5ng/ml) (15324505, MP Biomedical) as previously described (Feldman et al., 2017).

METHOD DETAILS

Flow cytometry, FACS, cell cycle, and proliferation analyses—Flow cytometry analyses were performed using live B cells (5×10^{-5}) washed in PBS plus 2% FCS, and stained with antibodies conjugated with specific fluorescent dyes (Resource Table) by gating for Fixable Viability Stain 510 (FVS510) (BD Biosciences) and/or forward- and side scatter on a CyAn ADP with Summit software (Becton Coulter, Indianapolis, IN), a CytoFLEX with CytoExpert software (Becton Coulter, Indianapolis, IN) or an Attune (Invitrogen, CA) with Flowjo software (Flowjo LLC, OR). To detect cytoplasmic IgE, B cells were incubated with soluble anti-IgE, then permeablized and fixed using the BD Cytofix/Cytoperm Fixation/Permeabilization Kit (BD Biosciences, San Diego, CA) and then stained with Bv510-anti-IgE as previously described (Wu et al., 2017).

FACS analyses were performed using a MoFlo Astrios supported by Summit software (Beckman Coulter, Indianapolis, IN) at the University of Illinois College of Medicine and BD FACS Aria Fusion or AriaIIIu (BD Biosciences, Franklin Lakes, NJ) supported by FACS DIVA software at the University of Chicago. CD43− naive B cells from heterozygous (C57BL/6 × BALB/c) Iε-tdTom mice were stained with anti-IgM^a (FITC) and anti-IgM^b (PE) and sorted for IgM^a and IgM^b B cells, respectively, and then were activated with NOT as described. B cells were monitored for cell division by carboxyfluoresceinsuccinimidyl ester dye (CFSE) (BD Biosciences, San Jose, CA) loss according to manufacture's instructions with modifications. Briefly, resting B cells were washed once with HBSS buffer, incubated with CFSE (1 μM) for 10 minutes at 37°C, washed in HBSS containing 0.5% FBS and an aliquot was immediately analyzed by flow cytometry. The remaining cells were activated in LPS for 3 days and analyzed for CFSE loss. Live cells were identified with FVS510, and analyzed for CD138-PE-Cy7, IgM-e450, IgD-PE, Igκ-PE-cf594 and Igλ-

Author Manuscript Author Manuscript Author Manuscript Author Manuscript

APC and IgM+IgD CD138−, IgM^{dim}IgD-CD138− and BCR-CD138− by flow cytometry on a CytoFLEX (Beckman Coulter, Indianapolis, IN) and data was analyzed using Kaluza software. Cell cycle analyses were performed on B cells activated with LPS for 3 days whereupon BCR-CD138− B cells were purified in two steps. First, cells were submitted to anti-IgM microbeads (MACS, Miltenyi) and the IgM^{-}/IgM^{dim} cells (flowthrough) were isolated. Second, live cells were identified with FVS510, and analyzed for CD138-PE-Cy7, IgM-e450, IgD-PE, IgG3− FITC, IgG2b-FITC, Igκ-PE-cf594 and Igλ-APC. BCR-CD138− and IgM^{dim}CD138− cells were purified by FACS and cultured with VybrantDyeCycle Violet Stain (5 μM) (Invitrogen, Eugene, OR) in RPMI culture medium at 37°C for 30 min and then analyzed by flow cytometry (CytoFLEX, Beckman Coulter, Indianapolis IN) supported by FlowJo software. Fluorescence microscopy was performed on a BZ-X710 analyzer (Keyance, Itasca, IL).

Quantitative RT-PCR—Real-time quantitative (q) RT-PCR was performed using a viiA7 system and SYBR Green PCR Mix (Applied Biosystems) as described (Wuerffel et al., 2007) except that primers for 18S rRNA were used (Rhinn et al., 2008) to normalize samples. Semiquantitative RT-PCR assays for circle transcripts (CT) were carried out using Phusion DNA polymerase (Thermo Fisher) (25 μl) at 98°C, 3 min for 1x; 98°C 10 s, 60°C 10 s, 72°C 15 s, for 31x, 33x and 35x and 7 ul were analyzed by gel electrophoresis. RT-PCR primers are listed in (Resource Table). Results represent the average of at least three independent experiments from 3–6 mice and each sample was assayed in duplicate or triplicate and SEMs were calculated.

3C library construction and analysis—Optimized 3C library construction and assays for the Igh locus using Hind III and Hind III+EcoRI were performed as described (Feldman et al., 2015; Feldman et al., 2017). A list of 3C primers and probes is provided (Resource Table). Briefly, splenic B cells that were resting-, or activated with LPS+IL4 for 40 hours were crosslinked using 1% formaldehyde. Template concentration using the Mb1 primers was determined as described (Wuerffel et al., 2007). Quantitative PCR (qPCR) for 3C was used in combination with 5′FAM and 3′BHQ1 modified probes (IDT) to detect of 3C products. A control template in which all possible 3C ligation products are present in equimolar concentration was used to control for differences in amplification efficiency between primer sets (Resource Table). The data were normalized using the interaction frequency between two fragments within the non-expressed *Amylase (Amy)* gene to facilitate sample to sample comparisons (Resource Table). The relative crosslinking frequency between two *Igh* restriction fragments was calculated: $X_{Igh} = [S_{Igh}/S_{Amy}]$ Cell Type/$[S_{Igh}/S_{Amy}]$ Control mix. S_{Igh} is the signal obtained using primer pairs for two different *Igh* restriction fragments and S_{Amy} is the signal obtained with primer pairs for the *GD* locus fragments. The crosslinking frequency for the *GD* fragments was arbitrarily set to a value of 1 to permit sample comparisons. Data are represented as mean ± SEM.

4C and 5C library construction and analysis—Construction of 4C libraries was adapted from methods described in (Stadhouders et al., 2014; van de Werken et al., 2012a). Briefly, CD43− resting splenic B cells or B cells activated with LPS+IL4 for 40 hours, and Rag2−/− pro-B cells that were cultured with IL7 as described (Montefiori et al.,

Author Manuscript Author Manuscript Author Manuscript Author Manuscript

2016) and splenic T cells that were enriched using the mouse T cell enrichment column kit (MTCC-5, R&D) and cultured with ConA (5ng/ml) (15324505, MP Biomedical) as previously described (Feldman et al., 2017) were crosslinked using 1% formaldehyde. Hind III and DpnII were used as the primary and secondary restriction enzymes, respectively for each of two biological replicates. Inverse PCR was performed using the Expand Long Template PCR System from two viewpoints with barcoded primers (Figure S1D). The PCR products were submitted to next-generation sequencing using an Illumina NextSeq 500 sequencer with 75 bp paired-end reads. Reads were trimmed and aligned to an *in silico* library constructed based on the mouse (*Mus musculus*) genome (mm9) and the approach outlined by van der Werken et al. (van de Werken et al., 2012a) and analyzed using the Tanay 4Cseq pipeline https://compgenomics.weizmann.ac.il/tanay/?page_id=367. 4C-seq library statistics are shown in (Figure S1E).

5C primers follow an alternating pattern and were designed at HindIII restriction sites using the 5C primer design tools that were previously reported (Kumar et al., 2013; Montefiori et al., 2016). 5C libraries were constructed using Hind III restriction sites and primers that were targeted to the Igh locus between coordinates chr12:114390223–117301828 (mm9), and a chromosome 5 gene desert (chr5:133194370–133464774 (mm9)) (Montefiori et al., 2016) and using chromatin from B cells that were resting- or activated with LPS+IL4 for 40 hours. The mouse embryonic fibroblasts (MEF) and Rag2−/−pro-B cells 5C libraries were previously reported (Montefiori et al., 2016). Primers settings were: U-BLAST: 3; S-BLAST: 80: 15-MER: 800; MIN_FSIZE: 1000; MAX_FSIZE: 15,000; OPT_TM: 65; OPT_PSIZE: 30. 5C products were analyzed by Solexa paired-end deep sequencing. A virtual genome of all potential 5C products was created using DNA sequence adjacent to Hind III restriction fragment sites. Reads were mapped to the virtual genome using Novoalign (http://www.novocraft.com) as previously reported (Kumar et al., 2013). Only paired-ends for which one end mapped to a forward primer and the other to a reverse primer were considered and reads that mapped to more than one location were discarded. The 5C library composition for each experiment constructed here is summarized in Figure S2B. 5C analyses were carried out on two biological replicates from cell types. In all cases the mappable reads were proportional to the degree of multiplexing, indicating equivalent library quality despite different read numbers. The heatmaps are scaled as follows: for Figure 1F, MEF 37–1840, Rag2−/− pro B cells: 19–1254, resting B cells: 89–6355 and LPS+IL4 B cells 19–1254.

QUANTIFICATION AND STATISTICAL ANALYSIS

P values were calculated by using two-tailed Student's t test. P values were represented as follows: $p > 0.05$ (*), $p > 0.01$ (**), $p > 0.001$ (***). P values were integrated into the Figure Legends and the Figures. Two biological replicates were analyzed for the 4C and 5C studies and each biological replicate was generated from B cell cultures pooled from 2–3 mice. All biological experiments are representative of at least three independent B cell cultures, each from an independent mouse. All RT-PCR studies were quantitated using at least three cDNA samples from independent B cell cultures and assayed in duplicate or triplicate. Data are represented as mean ± SEM.

Author Manuscript Author Manuscript Author Manuscript Author Manuscript

Supplementary Material

Refer to Web version on PubMed Central for supplementary material.

ACKNOWLEDGMENTS

This work was supported by grants to A.L.K. from the NIH (RO1AI121286, R21AI133050). We thank Drs. J. Stavnezer and R. Sen for helpful discussions.

REFERENCES

Benner C, Isoda T, and Murre C (2015). New roles for DNA cytosine modification, eRNA, anchors, and superanchors in developing B cell progenitors. Proc. Natl. Acad. Sci. USA 112, 12776–12781. [PubMed: 26417104]

Conrad DH, Keegan AD, Kalli KR, Van Dusen R, Rao M, and Levine AD (1988). Superinduction of low affinity IgE receptors on murine B lymphocytes by lipopolysaccharide and IL-4. J. Immunol 141, 1091–1097. [PubMed: 2969397]

Dekker J, and Mirny L (2016). The 3D genome as moderator of chromosomal communication. Cell 164, 1110–1121. [PubMed: 26967279]

Dixon JR, Selvaraj S, Yue F, Kim A, Li Y, Shen Y, Hu M, Liu JS, and Ren B (2012). Topological domains in mammalian genomes identified by analysis of chromatin interactions. Nature 485, 376–380. [PubMed: 22495300]

Dong J, Panchakshari RA, Zhang T, Zhang Y, Hu J, Volpi SA, Meyers RM, Ho YJ, Du Z, Robbiani DF, et al. (2015). Orientation-specific joining of AID-initiated DNA breaks promotes antibody class switching. Nature 525, 134–139. [PubMed: 26308889]

Dougier HL, Reynaud S, Pinaud E, Carrion C, Delpy L, and Cogné M (2006). Interallelic class switch recombination can reverse allelic exclusion and allow *trans*-complementation of an IgH locus switching defect. Eur. J. Immunol 36, 2181–2191. [PubMed: 16874738]

Dudley DD, Manis JP, Zarrin AA, Kaylor L, Tian M, and Alt FW (2002). Internal IgH class switch region deletions are position-independent and enhanced by AID expression. Proc. Natl. Acad. Sci. USA 99, 9984–9989. [PubMed: 12114543]

Feldman S, Achour I, Wuerffel R, Kumar S, Gerasimova T, Sen R, and Kenter AL (2015). Constraints contributed by chromatin looping limit recombination targeting during Ig class switch recombination. J. Immunol 194, 2380–2389. [PubMed: 25624452]

Feldman S, Wuerffel R, Achour I, Wang L, Carpenter PB, and Kenter AL (2017). 53BP1 contributes to *Igh* locus chromatin topology during class switch recombination. J. Immunol 198, 2434–2444. [PubMed: 28159901]

Fudenberg G, Imakaev M, Lu C, Goloborodko A, Abdennur N, and Mirny LA (2016). Formation of chromosomal domains by loop extrusion. Cell Rep 15, 2038–2049. [PubMed: 27210764]

Garrett FE, Emelyanov AV, Sepulveda MA, Flanagan P, Volpi S, Li F, Loukinov D, Eckhardt LA, Lobanenkov VV, and Birshtein BK (2005). Chromatin architecture near a potential 3′ end of the *Igh* locus involves modular regulation of histone modifications during B-cell development and in vivo occupancy at CTCF sites. Mol. Cell. Biol 25, 1511–1525. [PubMed: 15684400]

Gu H, Zou YR, and Rajewsky K (1993). Independent control of immunoglobulin switch recombination at individual switch regions evidenced through Cre-loxP-mediated gene targeting. Cell 73, 1155–1164. [PubMed: 8513499]

He JS, Meyer-Hermann M, Xiangying D, Zuan LY, Jones LA, Ramakrishna L, de Vries VC, Dolpady J, Aina H, Joseph S, et al. (2013). The distinctive germinal center phase of IgE^{+} B lymphocytes limits their contribution to the classical memory response. J. Exp. Med 210, 2755–2771. [PubMed: 24218137]

Hodgkin PD, Lee JH, and Lyons AB (1996). B cell differentiation and isotype switching is related to division cycle number. J. Exp. Med 184, 277–281. [PubMed: 8691143]

Iannelli F, Galbiati A, Capozzo I, Nguyen Q, Magnuson B, Michelini F, D'Alessandro G, Cabrini M, Roncador M, Francia S, et al. (2017). A damaged genome's transcriptional landscape

Author Manuscript Author Manuscript Author Manuscript Author Manuscript

through multilayered expression profiling around in situ-mapped DNA double-strand breaks. Nat. Commun 8, 15656. [PubMed: 28561034]

Jung S, Siebenkotten G, and Radbruch A (1994). Frequency of immunoglobulin E class switching is autonomously determined and independent of prior switching to other classes. J. Exp. Med 179, 2023–2026. [PubMed: 8195724]

Kaminski DA, and Stavnezer J (2007). Stimuli that enhance IgA class switching increase histone 3 acetylation at Sα, but poorly stimulate sequential switching from IgG2b. Eur. J. Immunol 37, 240–251. [PubMed: 17163453]

Kenter AL (2012). AID targeting is dependent on RNA polymerase II pausing. Semin. Immunol 24, 281–286. [PubMed: 22784681]

Khair L, Guikema JE, Linehan EK, Ucher AJ, Leus NG, Ogilvie C, Lou Z, Schrader CE, and Stavnezer J (2014). ATM increases activation-induced cytidine deaminase activity at downstream S regions during class-switch recombination. J. Immunol 192, 4887–4896. [PubMed: 24729610]

Kingzette M, Spieker-Polet H, Yam PC, Zhai SK, and Knight KL (1998). Trans-chromosomal recombination within the Ig heavy chain switch region in B lymphocytes. Proc. Natl. Acad. Sci. USA 95, 11840–11845. [PubMed: 9751752]

Kumar S, Wuerffel R, Achour I, Lajoie B, Sen R, Dekker J, Feeney AJ, and Kenter AL (2013). Flexible ordering of antibody class switch and V(D)J joining during B-cell ontogeny. Genes Dev 27, 2439–2444. [PubMed: 24240234]

Le Q, and Maizels N (2015). Cell cycle regulates nuclear stability of AID and determines the cellular response to AID. PLoS Genet 11, e1005411. [PubMed: 26355458]

Lieberman-Aiden E, van Berkum NL, Williams L, Imakaev M, Ragoczy T, Telling A, Amit I, Lajoie BR, Sabo PJ, Dorschner MO, et al. (2009). Comprehensive mapping of long-range interactions reveals folding principles of the human genome. Science 326, 289–293. [PubMed: 19815776]

Lorenz M, Jung S, and Radbruch A (1995). Switch transcripts in immunoglobulin class switching. Science 267, 1825–1828. [PubMed: 7892607]

Mandler R, Finkelman FD, Levine AD, and Snapper CM (1993). IL-4 induction of IgE class switching by lipopolysaccharide-activated murine B cells occurs predominantly through sequential switching. J. Immunol 150, 407–418. [PubMed: 8419474]

Manis JP, Morales JC, Xia Z, Kutok JL, Alt FW, and Carpenter PB (2004). 53BP1 links DNA damage-response pathways to immunoglobulin heavy chain class-switch recombination. Nat. Immunol 5, 481–487. [PubMed: 15077110]

Matsuoka M, Yoshida K, Maeda T, Usuda S, and Sakano H (1990). Switch circular DNA formed in cytokine-treated mouse splenocytes: Evidence for intramolecular DNA deletion in immunoglobulin class switching. Cell 62, 135–142. [PubMed: 2114219]

McIntyre TM, Kehry MR, and Snapper CM (1995). Novel in vitro model for high-rate IgA class switching. J. Immunol 154, 3156–3161. [PubMed: 7897205]

Misaghi S, Garris CS, Sun Y, Nguyen A, Zhang J, Sebrell A, Senger K, Yan D, Lorenzo MN, Heldens S, et al. (2010). Increased targeting of donor switch region and IgE in Sγ1-deficient B cells. J. Immunol 185, 166–173. [PubMed: 20511552]

Montefiori L, Wuerffel R, Roqueiro D, Lajoie B, Guo C, Gerasimova T, De S, Wood W, Becker KG, Dekker J, et al. (2016). Extremely long-range chromatin loops link topological domains to facilitate a diverse antibody repertoire. Cell Rep 14, 896–906. [PubMed: 26804913]

Muramatsu M, Kinoshita K, Fagarasan S, Yamada S, Shinkai Y, and Honjo T (2000). Class switch recombination and hypermutation require activation-induced cytidine deaminase (AID), a potential RNA editing enzyme. Cell 102, 553–563. [PubMed: 11007474]

Nagaoka H, Muramatsu M, Yamamura N, Kinoshita K, and Honjo T (2002). Activation-induced deaminase (AID)-directed hypermutation in the immunoglobulin Sμ region: Implication of AID involvement in a common step of class switch recombination and somatic hypermutation. J. Exp. Med 195, 529–534. [PubMed: 11854365]

Nasmyth K (2001). Disseminating the genome: Joining, resolving, and separating sister chromatids during mitosis and meiosis. Annu. Rev. Genet 35, 673–745. [PubMed: 11700297]

Nichols MH, and Corces VG (2015). A CTCF code for 3D genome architecture. Cell 162, 703–705. [PubMed: 26276625]

Author Manuscript Author Manuscript Author Manuscript Author Manuscript

Nora EP, Lajoie BR, Schulz EG, Giorgetti L, Okamoto I, Servant N, Piolot T, van Berkum NL, Meisig J, Sedat J, et al. (2012). Spatial partitioning of the regulatory landscape of the X-inactivation centre. Nature 485, 381–385. [PubMed: 22495304]

Otipoby KL, Waisman A, Derudder E, Srinivasan L, Franklin A, and Rajewsky K (2015). The B-cell antigen receptor integrates adaptive and innate immune signals. Proc. Natl. Acad. Sci. USA 112, 12145–12150. [PubMed: 26371314]

Pavri R, Gazumyan A, Jankovic M, Di Virgilio M, Klein I, Ansarah-Sobrinho C, Resch W, Yamane A, Reina San-Martin B, Barreto V, et al. (2010). Activation-induced cytidine deaminase targets DNA at sites of RNA polymerase II stalling by interaction with Spt5. Cell 143, 122–133. [PubMed: 20887897]

Pefanis E, Wang J, Rothschild G, Lim J, Chao J, Rabadan R, Economides AN, and Basu U (2014). Noncoding RNA transcription targets AID to divergently transcribed loci in B cells. Nature 514, 389–393. [PubMed: 25119026]

Petersen S, Casellas R, Reina-San-Martin B, Chen HT, Difilippantonio MJ, Wilson PC, Hanitsch L, Celeste A, Muramatsuk M, Pilch DR, et al. (2001). AID is required to initiate Nbs1/γ-H2AX focus formation and mutations at sites of class switching. Nature 414, 660–665. [PubMed: 11740565]

Pinaud E, Khamlichi AA, Le Morvan C, Drouet M, Nalesso V, Le Bert M, and Cogné M (2001). Localization of the 3′ IgH locus elements that effect long-distance regulation of class switch recombination. Immunity 15, 187–199. [PubMed: 11520455]

Pone EJ, Zhang J, Mai T, White CA, Li G, Sakakura JK, Patel PJ, Al-Qahtani A, Zan H, Xu Z, and Casali P (2012). BCR-signalling synergizes with TLR-signalling for induction of AID and immunoglobulin class-switching through the non-canonical NF-κB pathway. Nat. Commun 3, 767. [PubMed: 22473011]

Predeus AV, Gopalakrishnan S, Huang Y, Tang J, Feeney AJ, Oltz EM, and Artyomov MN (2014). Targeted chromatin profiling reveals novel enhancers in Ig H and Ig L chain Loci. J. Immunol 192, 1064–1070. [PubMed: 24353267]

Rao SS, Huntley MH, Durand NC, Stamenova EK, Bochkov ID, Robinson JT, Sanborn AL, Machol I, Omer AD, Lander ES, and Aiden EL (2014). A 3D map of the human genome at kilobase resolution reveals principles of chromatin looping. Cell 159, 1665–1680. [PubMed: 25497547]

Reina-San-Martin B, Chen J, Nussenzweig A, and Nussenzweig MC (2007). Enhanced intra-switch region recombination during immunoglobulin class switch recombination in 53BP1$^{-/-}$ B cells. Eur. J. Immunol 37, 235–239. [PubMed: 17183606]

Reynaud S, Delpy L, Fleury L, Dougier HL, Sirac C, and Cogné M (2005). Interallelic class switch recombination contributes significantly to class switching in mouse B cells. J. Immunol 174, 6176–6183. [PubMed: 15879114]

Rhinn H, Marchand-Leroux C, Croci N, Plotkine M, Scherman D, and Escriou V (2008). Housekeeping while brain's storming validation of normalizing factors for gene expression studies in a murine model of traumatic brain injury. BMC Mol. Biol 9, 62. [PubMed: 18611280]

Rowley MJ, and Corces VG (2018). Organizational principles of 3D genome architecture. Nat. Rev. Genet 19, 789–800. [PubMed: 30367165]

Sanborn AL, Rao SS, Huang SC, Durand NC, Huntley MH, Jewett AI, Bochkov ID, Chinnappan D, Cutkosky A, Li J, et al. (2015). Chromatin extrusion explains key features of loop and domain formation in wild-type and engineered genomes. Proc. Natl. Acad. Sci. USA 112, E6456–E6465. [PubMed: 26499245]

Schrader CE, Bradley SP, Vardo J, Mochegova SN, Flanagan E, and Stavnezer J (2003). Mutations occur in the Ig Sμ region but rarely in Sγ regions prior to class switch recombination. EMBO J 22, 5893–5903. [PubMed: 14592986]

Schrader CE, Guikema JE, Linehan EK, Selsing E, and Stavnezer J (2007). Activation-induced cytidine deaminase-dependent DNA breaks in class switch recombination occur during G1 phase of the cell cycle and depend upon mismatch repair. J. Immunol 179, 6064–6071. [PubMed: 17947680]

Sellars M, Reina-San-Martin B, Kastner P, and Chan S (2009). Ikaros controls isotype selection during immunoglobulin class switch recombination. J. Exp. Med 206, 1073–1087. [PubMed: 19414557]

Author Manuscript Author Manuscript Author Manuscript Author Manuscript

Sexton T, Yaffe E, Kenigsberg E, Bantignies F, Leblanc B, Hoichman M, Parrinello H, Tanay A, and Cavalli G (2012). Three-dimensional folding and functional organization principles of the *Drosophila* genome. Cell 148, 458–472. [PubMed: 22265598]

Shanbhag NM, Rafalska-Metcalf IU, Balane-Bolivar C, Janicki SM, and Greenberg RA (2010). ATM-dependent chromatin changes silence transcription in *cis* to DNA double-strand breaks. Cell 141, 970–981. [PubMed: 20550933]

Siebenkotten G, Esser C, Wabl M, and Radbruch A (1992). The murine IgG1/IgE class switch program. Eur. J. Immunol 22, 1827–1834. [PubMed: 1623926]

Stadhouders R, de Bruijn MJ, Rother MB, Yuvaraj S, Ribeiro de Almeida C, Kolovos P, Van Zelm MC, van Ijcken W, Grosveld F, Soler E, and Hendriks RW (2014). Pre-B cell receptor signaling induces immunoglobulin κ locus accessibility by functional redistribution of enhancer-mediated chromatin interactions. PLoS Biol 12, e1001791. [PubMed: 24558349]

Talay O, Yan D, Brightbill HD, Straney EE, Zhou M, Ladi E, Lee WP, Egen JG, Austin CD, Xu M, and Wu LC (2012). IgE^+ memory B cells and plasma cells generated through a germinal-center pathway. Nat. Immunol 13, 396–404. [PubMed: 22366892]

Ui A, Nagaura Y, and Yasui A (2015). Transcriptional elongation factor ENL phosphorylated by ATM recruits polycomb and switches off transcription for DSB repair. Mol. Cell 58, 468–482. [PubMed: 25921070]

van de Werken HJ, de Vree PJ, Splinter E, Holwerda SJ, Klous P, de Wit E, and de Laat W (2012a). 4C technology: Protocols and data analysis. Methods Enzymol 513, 89–112. [PubMed: 22929766]

van de Werken HJ, Landan G, Holwerda SJ, Hoichman M, Klous P, Chachik R, Splinter E, Valdes-Quezada C, Oz Y, Bouwman BA, et al. (2012b). Robust 4C-seq data analysis to screen for regulatory DNA interactions. Nat. Methods 9, 969–972. [PubMed: 22961246]

Vian L, Pękowska A, Rao SSP, Kieffer-Kwon KR, Jung S, Baranello L, Huang SC, El Khattabi L, Dose M, Pruett N, et al. (2018). The energetics and physiological impact of cohesin extrusion. Cell 173, 1165–1178.e20. [PubMed: 29706548]

Wang Q, Kieffer-Kwon KR, Oliveira TY, Mayer CT, Yao K, Pai J, Cao Z, Dose M, Casellas R, Jankovic M, et al. (2017). The cell cycle restricts activation-induced cytidine deaminase activity to early G1. J. Exp. Med 214, 49–58. [PubMed: 27998928]

Whyte WA, Orlando DA, Hnisz D, Abraham BJ, Lin CY, Kagey MH, Rahl PB, Lee TI, and Young RA (2013). Master transcription factors and mediator establish super-enhancers at key cell identity genes. Cell 153, 307–319. [PubMed: 23582322]

Wu YL, Stubbington MJ, Daly M, Teichmann SA, and Rada C (2017). Intrinsic transcriptional heterogeneity in B cells controls early class switching to IgE. J. Exp. Med 214, 183–196. [PubMed: 27994069]

Wuerffel RA, Du J, Thompson RJ, and Kenter AL (1997). Ig Sγ3 DNAspecifc double strand breaks are induced in mitogen-activated B cells and are implicated in switch recombination. J. Immunol 159, 4139–4144. [PubMed: 9379005]

Wuerffel R, Wang L, Grigera F, Manis J, Selsing E, Perlot T, Alt FW, Cogne M, Pinaud E, and Kenter AL (2007). S-S synapsis during class switch recombination is promoted by distantly located transcriptional elements and activation-induced deaminase. Immunity 27, 711–722. [PubMed: 17980632]

Xiong H, Dolpady J, Wabl M, Curotto de Lafaille MA, and Lafaille JJ (2012). Sequential class switching is required for the generation of high affinity IgE antibodies. J. Exp. Med 209, 353–364. [PubMed: 22249450]

Xue K, Rada C, and Neuberger MS (2006). The in vivo pattern of AID targeting to immunoglobulin switch regions deduced from mutation spectra in *msh2*$^{-/-}$ *ung*$^{-/-}$ mice. J. Exp. Med 203, 2085–2094. [PubMed: 16894013]

Yoshida K, Matsuoka M, Usuda S, Mori A, Ishizaka K, and Sakano H (1990). Immunoglobulin switch circular DNA in the mouse infected with Nippostrongylus brasiliensis: Evidence for successive class switching from mu to epsilon via gamma 1. Proc. Natl. Acad. Sci. USA 87, 7829–7833. [PubMed: 2122447]

Author Manuscript Author Manuscript Author Manuscript Author Manuscript

Zhang T, Franklin A, Boboila C, McQuay A, Gallagher MP, Manis JP, Khamlichi AA, and Alt FW (2010). Downstream class switching leads to IgE antibody production by B lymphocytes lacking IgM switch regions. Proc. Natl. Acad. Sci. USA 107, 3040–3045. [PubMed: 20133637]

Zhang X, Zhang Y, Ba Z, Kyritsis N, Casellas R, and Alt FW (2019). Fundamental roles of chromatin loop extrusion in antibody class switching. Nature 575, 385–389. [PubMed: 31666703]

Zheng S, Vuong BQ, Vaidyanathan B, Lin JY, Huang FT, and Chaudhuri J (2015). Non-coding RNA generated following lariat debranching mediates targeting of AID to DNA. Cell 161, 762–773. [PubMed: 25957684]

Author Manuscript Author Manuscript Author Manuscript Author Manuscript

Highlights

- Loop extrusion drives germline transcript promoter-enhancer contacts during CSR
- Promoter-promoter-3′ enhancer contacts mediate reverse sequential switching
- Use of the three CSR pathways is mouse strain- and Ig isotype-specific
- During CSR B cells become surface BCR^{neg} then re-express IgM or a switched isotype

Author Manuscript
Author Manuscript
Author Manuscript
Author Manuscript

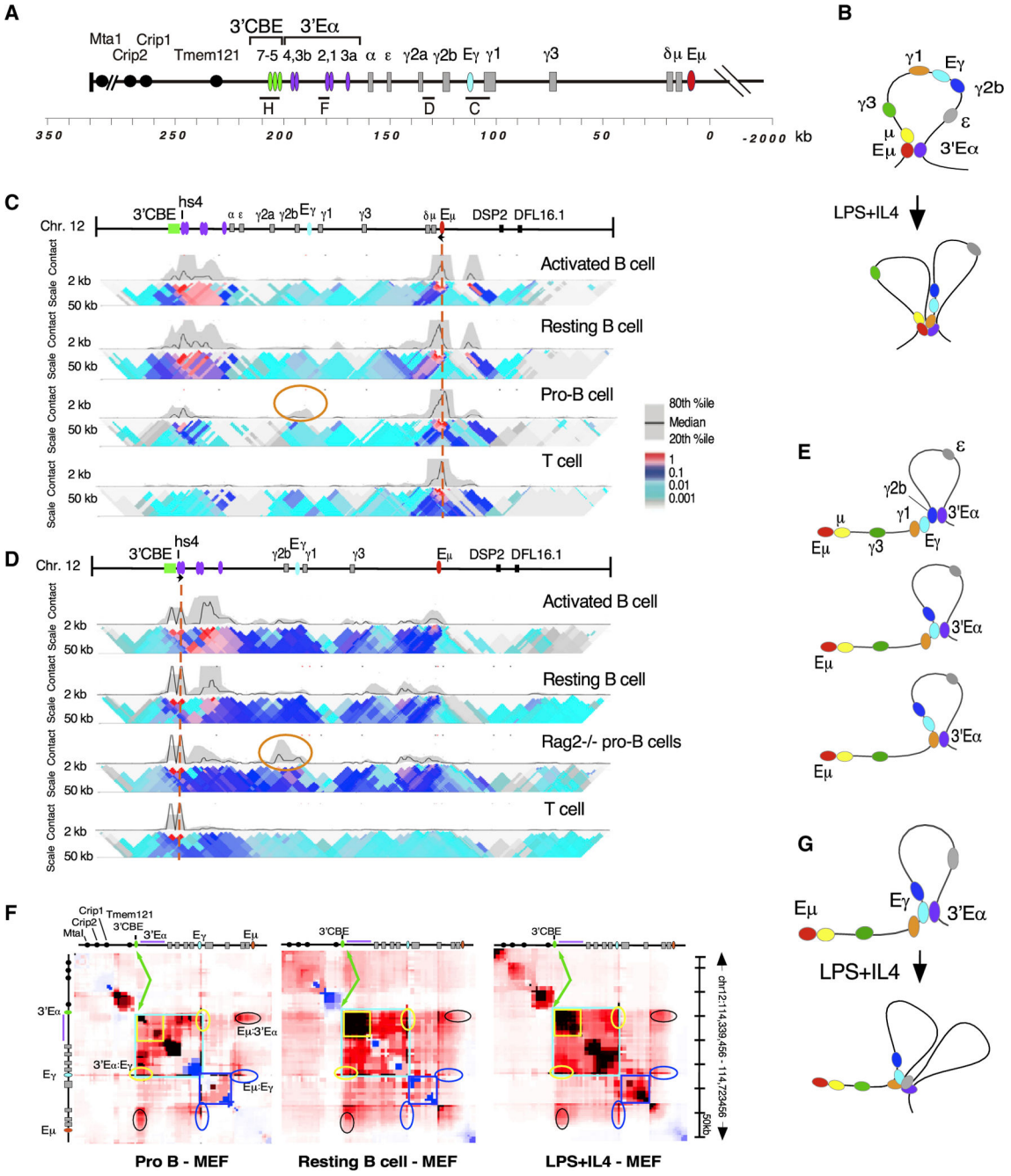

Figure 1. 3′Eα engages in asymmetric loop extrusion and anchors downstream GLT promoters

(A) Diagram of the C57BL/6 3′Igh locus oriented along the chromosome to scale. Eμ (orange oval), Eγ (teal oval), 3′Eα (purple ovals), CTCF binding elements (CBEs) (green ovals) at the 3′ boundary, C_H genes (gray rectangles), and genes outside the Igh locus (black circles) are shown. HindIII fragments (C, D, F, and H) for 3C assays are noted.

(B) The Eμ:3′Eα loop in resting B cells. The Eμ:3′Eα:γ1 loop upon LPS+IL-4 activation is shown.

Author Manuscript Author Manuscript Author Manuscript Author Manuscript

(C and D) 4C-seq contact profiles using a 10-kb window in the main trend subpanel were an average of two biological replicates. Viewpoint positions (dashed vertical red lines) at Eμ and 3′Eα hs4 with the Igh locus are shown at the top.

(E) Chromatin loops γ2b:hs4, Eγ:hs4, and γ1:hs4.

(F) Diagram of Eμ to the MtaI gene to scale (top left) with genomic coordinates (chr12, mm9) (y axis, right side). Difference plots (B cell minus MEF) were calculated using normalized 5C signals (150-kb bins, 15-kb step) that were averaged from two biological replicates. 5C reads in B cells (red intensities) or MEF (blue intensities) or constitutive (white) are shown. Igh TAD boundary is indicated by green arrows. Chromatin interactions within 3′Eα (yellow box), Eγ−3′Eα (teal box), Eγ:γ3 (blue box). Eμ:3′Eα (black oval), Eγ:3′Eα (yellow oval), and Eγ:Eμ (blue oval) interactions are shown.

(G) (Top) Eγ:3′Eα chromatin loop in resting B cells. (Bottom) Eγ:3′Eα:γ1:ε interactions following LPS+IL-4 treatment.

Author Manuscript Author Manuscript Author Manuscript Author Manuscript

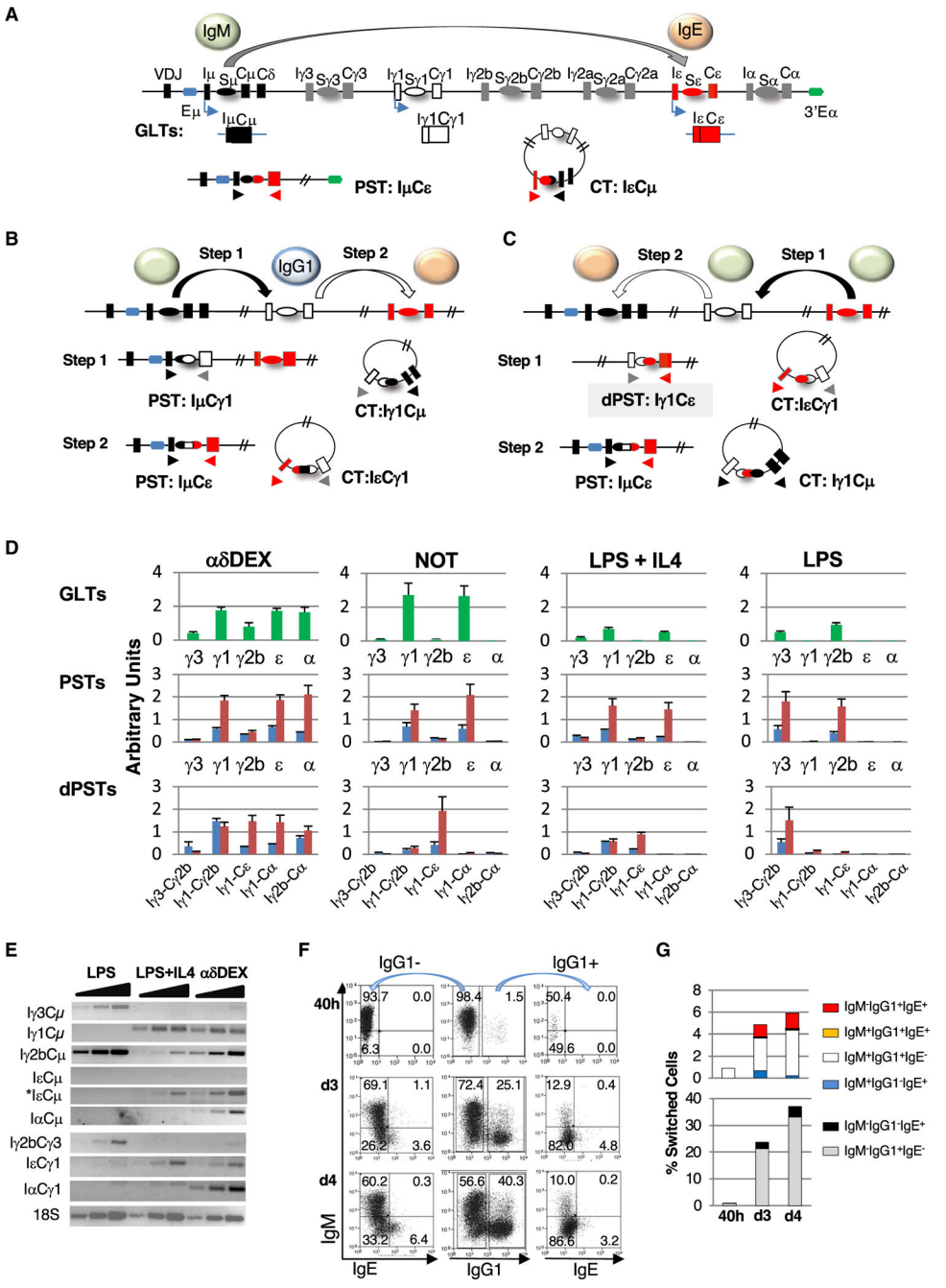

Figure 2. An alternative pathway for IgE switching in activated B cells

(A) Schematic of the Igh locus. Direct IgE switching generates a Sμ-Sε hybrid junction on the chromosome, an Sε-Sμ excision circle, and leads to IμCε PST and IεCμ CT expression. Ig surface expression: IgM^+ (green circle), IgE^+ cells (orange circle).

(B) Sequential IgE switching. Step 1 generates a Sμ-Sγ1 hybrid junction, an Sγ1-Sμ excision circle, and expression of IμCγ1 PSTs and Iγ1Cμ CTs. Ig surface expression: IgM^+, and $IgG1^+$ B cells. Step 2 produces a Sμ-Sγ1-Sε junction, Sε-Sγ1-Sμ excision circle, and expression of IμCε PSTs and IεCγ1 CTs. Ig surface expression: $IgG1^+$, IgE^+.

Author Manuscript Author Manuscript Author Manuscript Author Manuscript

(C) Reverse sequential switching. Step 1 includes production of Sγ1-Sε hybrid junctions and expression of Iγ1Cε dPST and IεCγ1 CT. Ig surface expression: $IgM1^+$. Step 2 forms Sμ-Sγ1-Sε hybrid junctions and expression of PST IμCε and CT Iγ1Cμ. Ig surface expression: IgM^+, IgE^+.

(D–G) Data were averaged from at least three independent B cell cultures and samples were tested in duplicate.

(D) Resting $M1'GFP^+$ B cells activated as indicated. qRT-PCR analyses of GLTs, PSTs, and dPSTs from B cells activated for 40 h (green bars), 3 days (d3, blue bars), and 4 days (d4, red bars) are shown with SEM.

(E) Semiquantitative RT-PCR for CTs from B cells activated for 4 days, as indicated.

(F) B cells activated with NOT for 40 h (40h; n = 3), 3 days (d3; n = 6), or 4 days (d4; n = 2) (number of mice, n). Representative plots of gated $IgG1^-$ and $IgG1^+$ cells were analyzed for surface IgM and cytoplasmic IgE.

(G) Quantitation of B cells expressing surface IgM, IgG1, and cytoplasmic IgE shown in (F).

Author Manuscript Author Manuscript Author Manuscript Author Manuscript

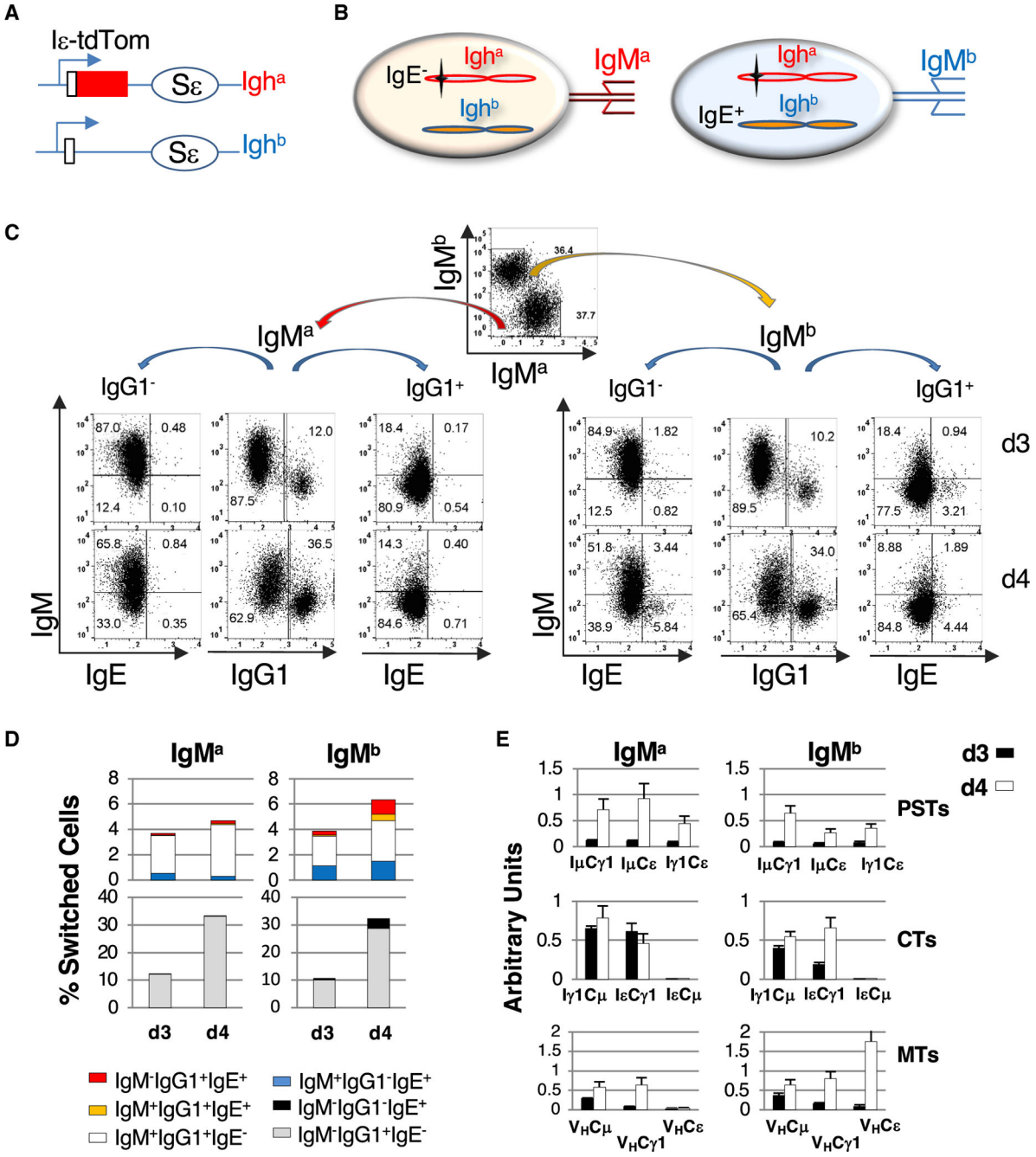

Figure 3. Reverse sequential switching occurs on the productively rearranged allele

B cell cultures were derived from at least three independent mice, and all PCR assays were tested in triplicate.

(A) A tdTom gene downstream of the Iε exon (Iε-tdTom) on the Igh^a allele (Wu et al., 2017). The Igh^b allele is WT.

(B) BALB/$c^{Iε\text{-}tdTom}$ Ig^a allele: td-Tom insertion (black cruciform) fails to express IgE. C57BL/6 Ig^b allele is proficient for IgE switching.

Author Manuscript Author Manuscript Author Manuscript Author Manuscript

(C) IgM^a (red arrow) and IgM^b (yellow arrow) B cells were isolated and activated with NOT for 3 days (d3) and 4 days (d4). Representative plots show B cells gated for $IgG1^-$ and $IgG1^+$ and assessed for surface IgM and cytoplasmic IgE.
(D) The frequencies of Igh^a and Igh^b B cells expressing $IgG1^-$ and $IgG1^+$ in combination with IgM and IgE were averaged from three to six mice; results are arranged as stacks.
(E) qRT-PCR of PSTs, dPSTs, CTs, and MTs. SEM are shown.

Author Manuscript Author Manuscript Author Manuscript Author Manuscript

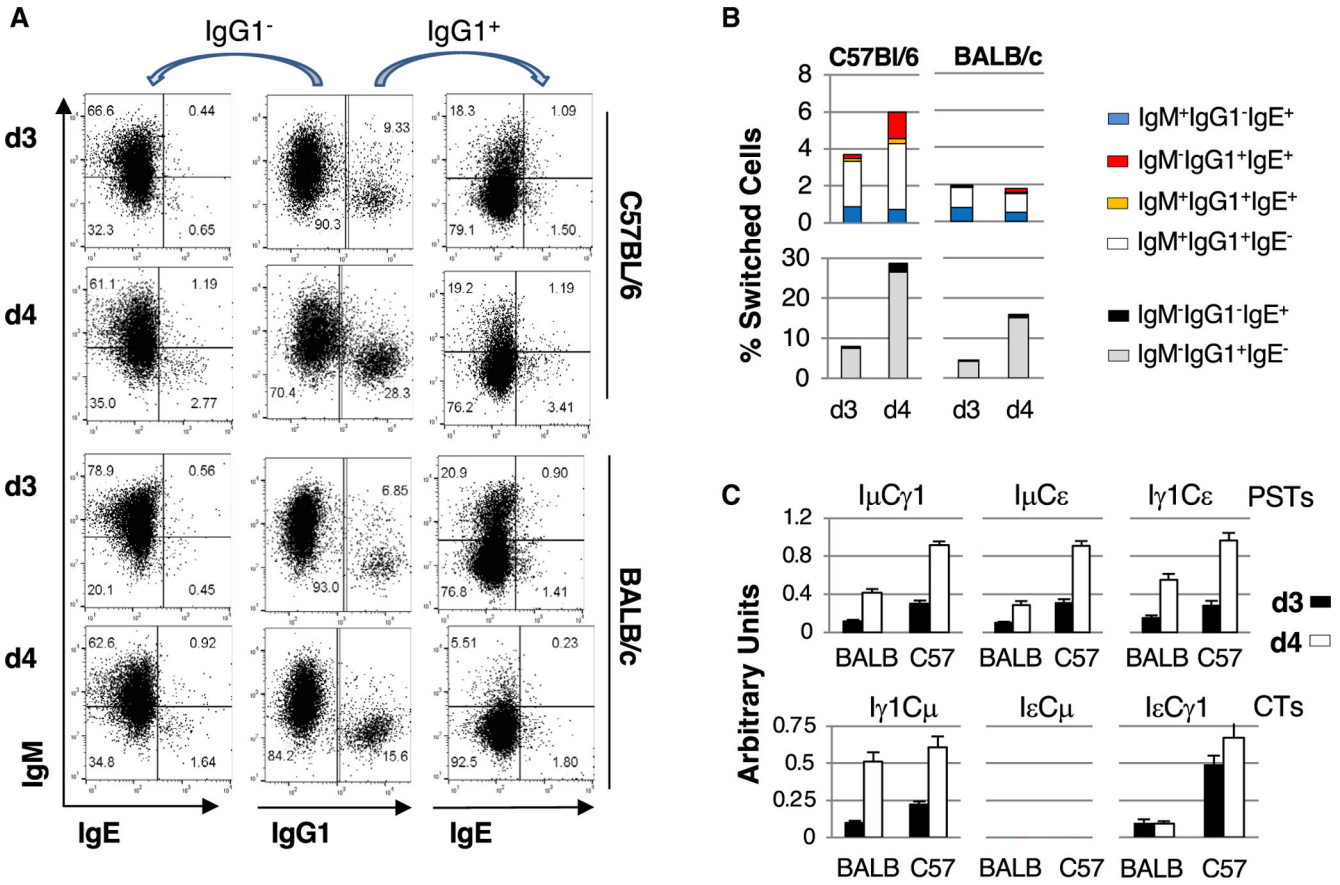

Figure 4. Reverse sequential switching is dominant in BALB/c mice

Resting splenic B cells from C57BL/6 and BALB/c mice were activated with NOT for 3 days (d3) and 4 days (d4) from at least three independent mice, and all PCR assays were tested in triplicate.

(A) Representative plots of activated B cells gated for $IgG1^{-}$ and $IgG1^{+}$ and then assessed for surface IgM and cytoplasmic IgE.

(B) The frequencies of B cells expressing $IgG1^{-}$ and $IgG1^{+}$ in combination with surface IgM and cytoplasmic IgE were averaged from three to six mice; results are arranged as stacks.

(C) qRT-PCR analyses of PST,s dPSTs, and CTs from B cells activated for 3 days (d3, filled bars) and 4 days (d4, open bars). SEM are shown.

Author Manuscript Author Manuscript Author Manuscript Author Manuscript

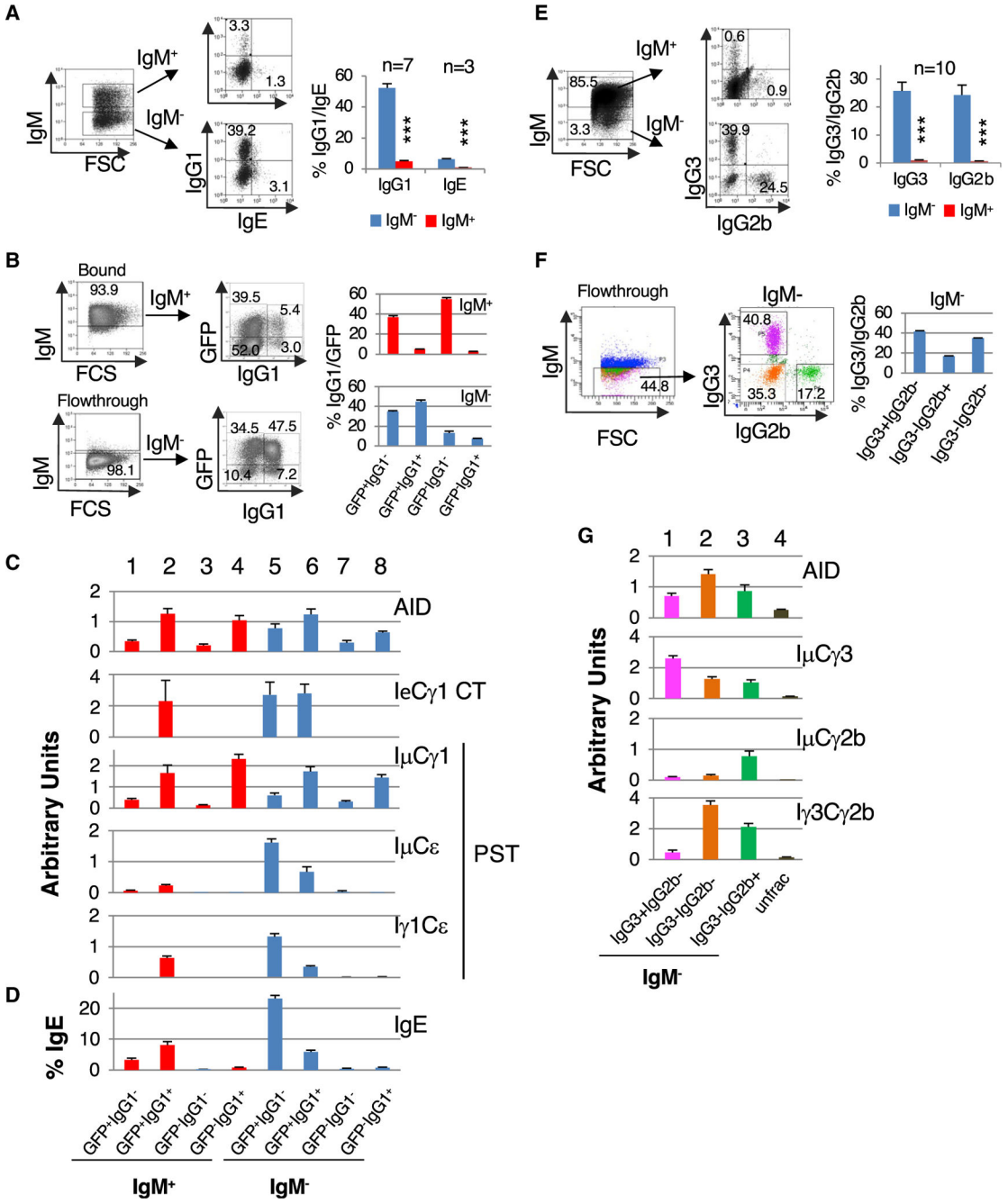

Figure 5. Downstream PSTs are enriched in IgM^{-}IgG^{-} B cells

B cells from M1′GFP^{+} (A–D) or C57BL/6 (E–G) mice were activated with NOT or LPS, respectively. B cell cultures were from at least three independent mice and all PCR assays were tested in triplicate.

(A and E) (Left panels) Representative plots of B cells were gated for IgM^{+} and IgM^{-} and then for IgG1 and IgE (A), or IgG3 and IgG2b (E) by flow cytometry on day 3 of cell stimulation. (Right panels) The frequency of IgG1^{+} and IgE^{+} (A) or IgG3^{+} and IgG2b^{+} (E) B cells in IgM^{+} (red bar) and IgM^{-} (blue bar) subpopulations was quantitated; SEMs are shown. Mice tested (n). P values (0.001, ***) from two tailed Student's t test.

Author Manuscript Author Manuscript Author Manuscript Author Manuscript

(B–D) B cells activated with NOT for 4 days were purified using anti-IgM beads, and IgM^+ (bound) and IgM^- (flowthrough) B cells were collected. (B) Cells were FACS purified based on surface IgM, IgG1, and GFP; the percentages of cells in each quadrant are noted. (C) qRT-PCR for PSTs, dPSTs, and AID. (D) B cells were analyzed by flow cytometry for surface IgM and IgG1 and cytoplasmic for IgE. The percentage of IgE^+ B cells is a fraction of each cell subset.

(F) IgM^- B cells (flowthrough) were further purified by FACS based on surface IgM, IgG3, and IgG2b. The percentage of IgM^-, IgM^-IgG3^+, and IgM^-IgG2b^+ cells is shown.

(G) qRT-PCR was performed on cDNAs prepared in (F).

Author Manuscript Author Manuscript Author Manuscript Author Manuscript

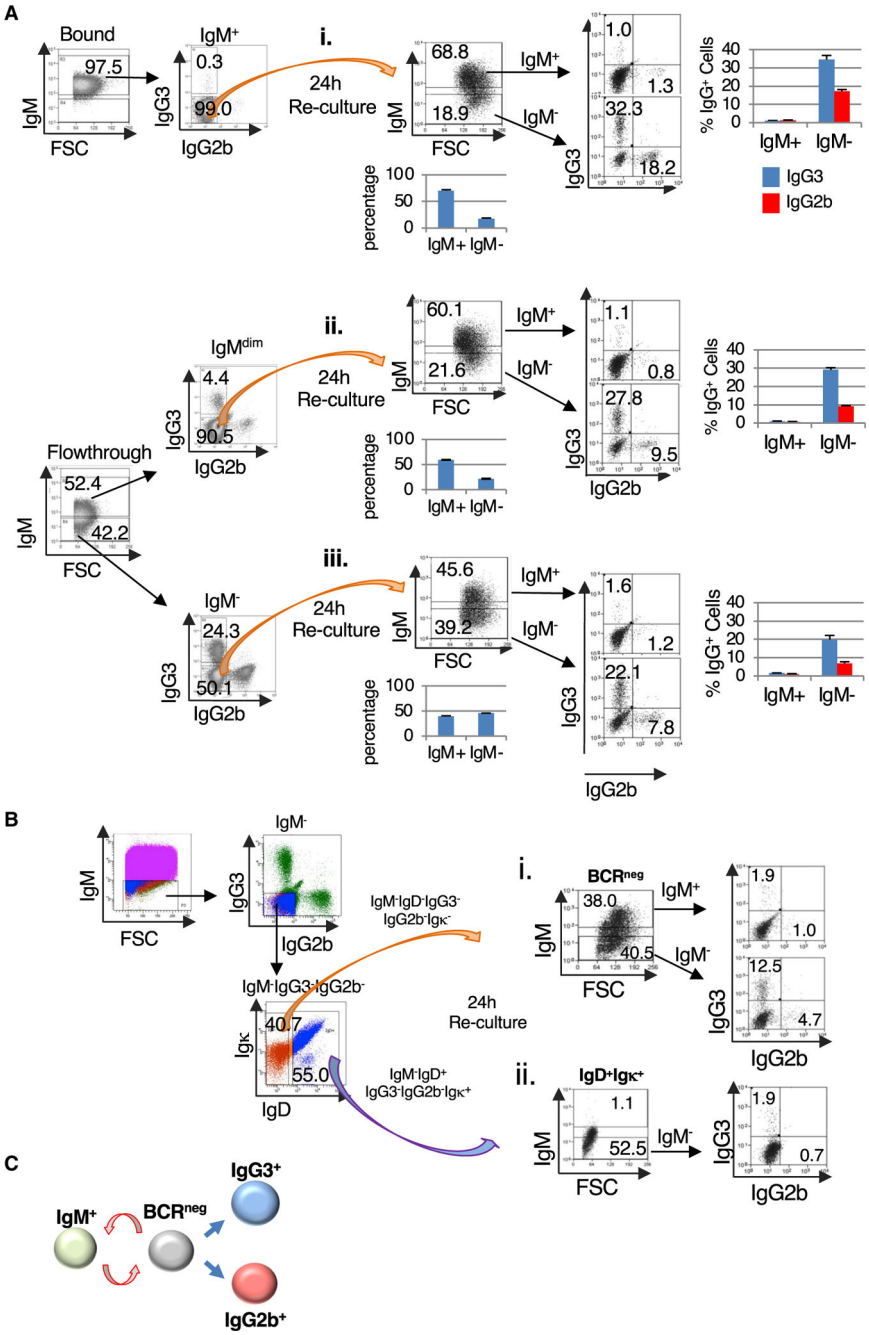

Figure 6. Switching B cells dynamically cycle through a BCR^{neg} state

All B cell cultures were derived from at least three independent mice.

(A) C57BL/6 resting splenic B cells were activated with LPS for 3 days, and IgM^{+} (bound) and IgM^{dim}/IgM^{-} (flowthrough) B cells were isolated and analyzed using anti-IgM-eFluor 450 (e450), anti-IgG3-Brilliant Violet 510 (BV510), and anti-IgG2b-FITC. (Left panels) IgM^{+}IgG3^{-}IgG2b^{-} cells (i), IgM^{dim}IgG3^{-}IgG2b^{-} cells (ii), andIgM^{-}IgG3^{-}IgG2b^{-} cells (iii) were FACS purified and re-cultured in LPS for 24 h (orange arrows). (Middle panels) Re-cultured cells were analyzed for IgM^{+}, IgM^{-}, and then for IgG3^{+}, IgG2b^{+} cells. (Right

Author Manuscript Author Manuscript Author Manuscript Author Manuscript

panels) Quantitation of $IgG3^+$ and $IgG2b^+$ B cells from IgM^+ and IgM^- subsets with SEMs shown.

(B) FACS gating strategy to isolate $IgM^-IgG3^-IgG2b^-IgD^-Ig\kappa^-$ (BCR^{neg}) and $IgM^-IgG3^-IgG2b^-IgD^+Ig\kappa^+$ ($IgD^+Ig\kappa^+$) B cells. BCR^{neg} (orange arrow) and $IgD^+Ig\kappa^+$ (blue arrow) were re-cultured in LPS for 24 h and analyzed for surface IgM, IgG3, and IgG2b.

(C) B cells dynamically transition between IgM^+ and BCR^{neg} states.

Author Manuscript Author Manuscript Author Manuscript Author Manuscript

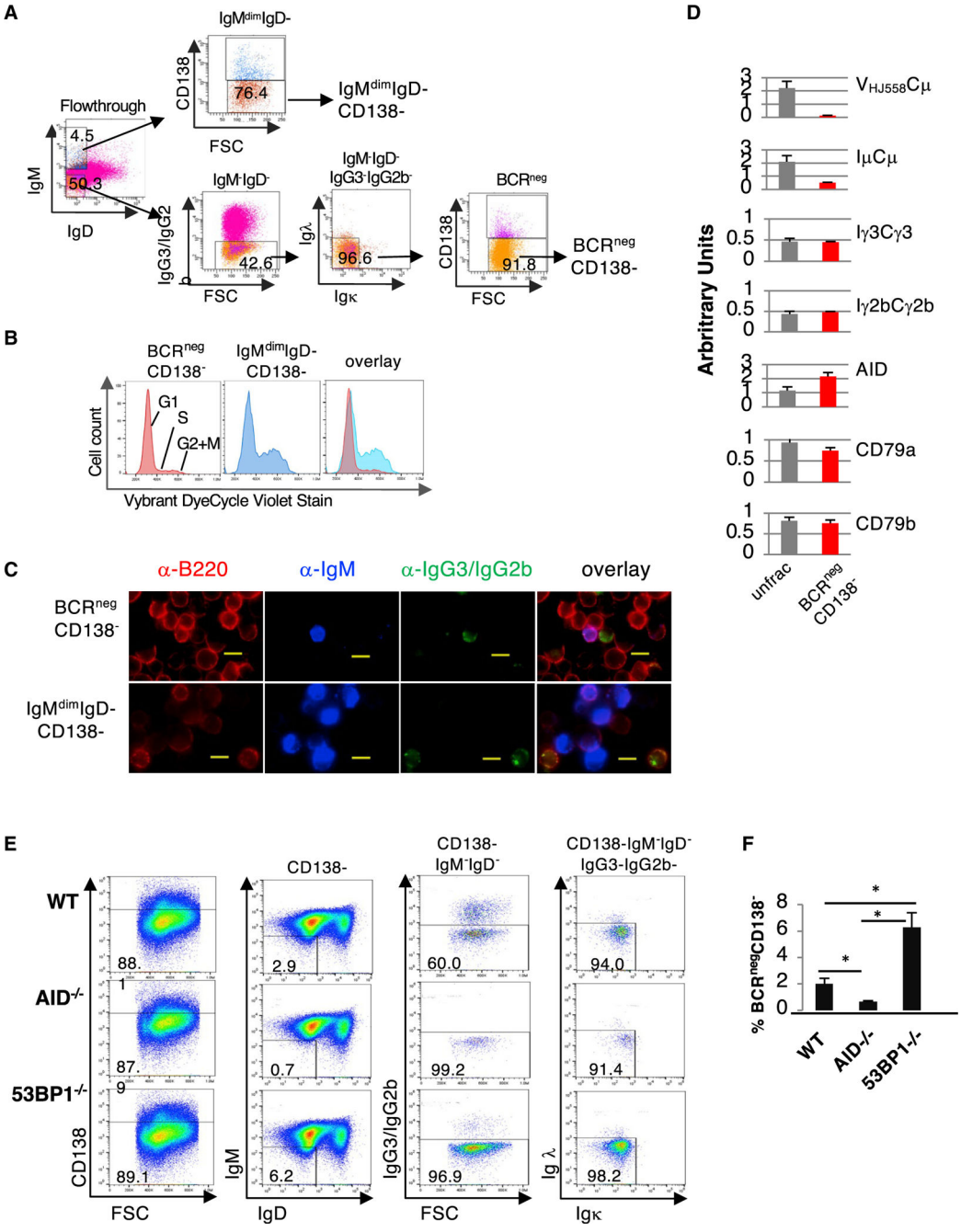

Figure 7. Transcriptional silencing of the μ locus favors downstream CSR in BCR^{neg} B cells

(A–C) Results are representative of least three independent experiments. C57BL/6 (A–E) AID$^{-/-}$ and 53BP1$^{-/-}$ (E) resting splenic B cells were activated with LPS for 3 days and IgM^{dim}/IgM^{-} (flowthrough) B cells were isolated (A–D).

(A) FACS gating strategy to purify IgM^{dim}IgD^{-}CD138^{-} and BCR^{neg}CD138^{-} cells using anti-IgM (e450), anti-IgD (phycoerythrin [PE]), anti-IgG3/anti-IgG2b (FITC), anti-Igk (PE-CF594), and anti-CD138 (PE-Cy7).

(B) IgM^{dim}IgD^{-}CD138^{-} and BCR^{neg}CD138^{-} cells were stained with Vybrant DyeCycle violet stain and cell cycle phases are shown.

Author Manuscript Author Manuscript Author Manuscript Author Manuscript

(C) $IgM^{dim}IgD^{-}CD138^{-}$ and $BCR^{neg}CD138^{-}$ B cells were fixed, permeabilized, stained with anti-B220 (PE, red), anti-IgM (e450, blue), and anti-IgG3/anti-IgG2b (FITC, green), and examined by fluorescence microscopy. Scale bars, 10 μm.

(D) qRT-PCR for transcripts from $BCR^{neg}CD138^{-}$ and $IgM^{dim}IgD^{-}CD138^{-}$ B cells and PCR assays were tested in triplicate and averaged, and SEMs are shown.

(E) Activated B cells were gated for $CD138^{-}IgM^{-}IgD^{-}IgG3IgG2b^{-}Ig\kappa^{-}Ig\lambda^{-}$ ($CD138^{-}BCR^{neg}$) B cells.

(F) The frequency of $CD138^{-}BCR^{neg}$ B cells is calculated as a percentage and was an average of live cells from three independent experiments with SEMs shown. P ≤ values (p % 0.05, *) from two tailed Student's t test.

Author Manuscript Author Manuscript Author Manuscript Author Manuscript

KEY RESOURCES TABLE

REAGENT or RESOURCE	SOURCE	IDENTIFIER
Antibodies		
anti-B220-PE	BD Biosciences	Cat# RA3-6B2; RRID: AB_394619
anti-IgM-e450	eBioscience	b121-15F9; RRID: AB_10671539
anti-IgG3-FITC	BD Biosciences	R40-82; RRID: AB_394840
anti-IgG3-Bv510	BD Biosciences	R40-82; RRID: AB_2742023
anti-IgG2b-FITC	BioLegend	RMG2b-1; RRID: AB_493297
anti-IgG1-FITC	BD PharMingen	A85-1; RRID: AB_394862
anti-IgG1-APC	BD PharMingen	A85-1; RRID: AB_1645625
anti-IgE	BD Biosciences	R35-72; RRID: AB_394846
anti-IgE-Bv510	BD Biosciences	R35-72; RRID: AB_2872207
anti-IgD-PE	Southern Biotech	11-26; RRID: AB_2794610
anti-Igλ-APC	BioLegend	RML-42; RRID:AB_961363
anti-Igκ- PE-CF594	BD Biosciences	187.1; RRID: AB_11153678
anti-CD138- PE-Cy7	BioLegend	281-2; RRID: AB_2562197
anti-IgM^a-FITC	BD PharMingen	DS-1; RRID: AB_394897
anti-IgM^b-PE	BD PharMingen	AF6-78; RRID: AB_394902
Chemicals, peptides, and recombinant proteins		
Fixable Viability Stain 510 (FVS-510)	BD Horizon ™	Cat # 564406
CFSE	BD Biosciences	Cat # 565082
Vybrant DyeCycle Violet Stain	Invitrogen	Cat # V35003
LPS	Sigma	Cat # 6511
Anti-IgD-dex	Fina Biosolutions	11-26c.2a
ConA	MP Biomedical	Cat # 15324505
rmIL4	R&D Systems	Cat # 404-ML/CF
IL5	BD Biosciences	Cat # 554581
RhTGFβ1	R&D Systems	Cat # 240-B002/CF
ConA	MP Biomedical	Cat # 15324505
Trizol	Invitrogen	Cat # 15596026
Phusion DNA polymerase	Thermo Fisher	Cat # F-530S
Expand Long Template PCR System	Sigma	Cat # 11681834001
Fast Syber Green Master Mix	Applied Biosystems/Thermo Fisher Scientific	Cat # 4385612
37% Formaldehyde	Fisher Scientific	Cat # BP531-25
Deposited data		
4C_seq data	GEO accession number	GSE183006
5C datasets – LPS+IL4 activated	GEO accession number	GSE183195
5C datasets – Resting splenic B cells	GEO accession number	GSE183574
Experimental models: Organisms/strains		
C57BL/6 mice	Jackson Labs	N/A
BALB/c	Jackson Labs	N/A

Author Manuscript Author Manuscript Author Manuscript Author Manuscript

REAGENT or RESOURCE	SOURCE	IDENTIFIER
Aicda−/−	Muramatsu et al., 2000	N/A
Iε-tdTom	Wu et al., 2017	N/A
M1 prime GFP^{+} knockin mice	Talay et al., 2012	N/A
53BP1$^{-/-}$ mice		N/A
Oligonucleotides		
Oligonucleotides (See Table S1)	This paper	N/A
Iγ2b F5′-CTA CCT GCA ACC TGG TGC-3′	This paper	N/A
Cγ2b R 5′-GGA ACC AGT TGT ATC TCC ACA CC-3′	This paper	N/A
Iε F 5′-CAG AAG ATG GCT TCG AAT AAG AAC A-3′	Kumar et al., 2013	N/A
Cε R 5′-CAG TGC CTT TAC AGG GCT TC-3′	This paper	N/A
Iγ1 F 5′- AGG AAT GTG TTT GGC ATG GAC-3′	Kumar et al., 2013	N/A
Cγ1 R 5′-ATG GAG TTA GTT TGG GCA GCA G-3′	This paper	N/A
Iγ3 F 5′-TGT CTG GAA GCT GGC AGG A-3′	Kumar et al., 2013	N/A
Cγ3 R 5′-GAT CCA GAT GTG TCA CCG C-3′	This paper	N/A
Iμ F 5′-TCC ACA CAA AGA CTC TGG ACC-3′	This paper	N/A
Cμ R 5′-TCA GTG TTG TTC TGG TAG TTC CAG-3′	This paper	N/A
Software and algorithms		
4C pipeline	https://compgenomics.weizmann.ac.il/tanay/?page_id=367	van de Werken et al., 2012a
Flowjo	Flowjo (version: v10.7.1)	N/A
Novoalign	http://www.novocraft.com	N/A
Other		
CD43 (Ly-48) Microbeads	Miltenyi Biotec	Cat# 130-049-801
Anti-IgM Microbeads	Miltenyi Biotec	Cat# 130-047-301
T cell enrichment column kit	R&D Systems	Cat# MTCC-5
BD Cytofix/Cytoperm Fixation/Permeabilization Kit	BD Biosciences	Cat# 554714